ChemComm

Accepted Manuscript

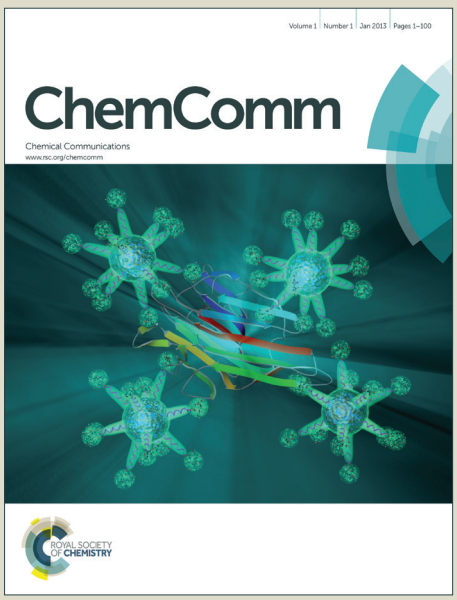

ROYAL SOCIETY OF CHEMISTRY

www.rsc.org/chemcomm

Cite this: DOI: 10.1039/c0xx00000x

www.rsc.org/xxxxxx

ARTICLE TYPE

Environmentally-benign catalysts for the selective catalytic reduction of NO_x from diesel engines: Structure-activity relationship and reaction mechanism aspects

Fudong Liu†, Yunbo Yu† and Hong He*

Received (in XXX, XXX) Xth XXXXXXXXX 20XX, Accepted Xth XXXXXXXXX 20XX
DOI: 10.1039/b000000x

Selective catalytic reduction of NO_x with NH_3 or hydrocarbons (NH_3-SCR or HC-SCR) in oxygen-rich exhaust from diesel engines remains a major challenge in environmental catalysis. The development of highly efficient, stable and environmentally-benign catalysts for SCR processes is very important for practical use. In this feature article, the structure-activity relationship of vanadium-free catalysts in NH_3-SCR reaction is discussed in detail, including Fe-, Ce-based oxide catalysts and Fe-, Cu-based zeolite catalysts, which is beneficial for catalyst redesign and activity improvement. Based on our research, a comprehensive mechanism contributing to the performance of Ag/Al_2O_3 in HC-SCR is provided, giving a clue to the design of a catalytic system with high efficiency.

1. Introduction

Nitrogen oxides (NO_x) are a major air pollutant that can lead to the formation of acid rain, photochemical smog and haze, thus endangering the eco-environment and human health [1]. The NO_x emissions resulting from human activity can be ascribed to stationary sources such as coal-fired power plants and mobile sources such as motor vehicles [2]. With the challenges arising from the energy crisis and global warming, the wide application of diesel engines in vehicles becomes more and more important because of their high fuel efficiency. Two main pollutants from diesel engine exhaust are NO_x and particulate matter (PM). Through the adjustment of heavy-duty diesel engines, the PM emission from diesel engines can be effectively reduced. However, due to the well-known "trade-off" relationship between PM and NO_x emitted from diesel engines, the increasing demand to eliminate NO_x, especially in oxygen-rich conditions, has drawn great attention from both academia and industry [3, 4]. Selective catalytic reduction (SCR) of NO_x using reductants such as NH_3, urea or hydrocarbons (HC) in the oxygen-rich exhausts is a highly efficient way to reduce NO_x emission, although it remains one of the major challenges in the field of environmental catalysis.

The SCR of NO_x with NH_3 (NH_3-SCR) was initially applied in the removal of NO_x from stationary sources, and the commercially used catalyst systems are mainly WO_3 or MoO_3 doped V_2O_5/TiO_2 [5, 6]. Vanadium-based NH_3-SCR catalysts have also been successfully used for the deNO_x process from diesel engines, starting in 2005 [7, 8]. However, disadvantages remain for the vanadium-based catalysts, including the toxicity of V_2O_5, the narrow operation temperature window, the easy sublimation of V_2O_5 and phase transformation of the TiO_2 support from anatase to rutile at high temperatures, which greatly restrict their further application, especially when stricter regulations are established for both PM and NO_x for diesel engines, and the SCR converter should be installed downstream of the diesel particulate filter (DPF), with timed thermal shock (~ 800 °C) in the regeneration processes of the DPF system. Therefore, many researchers are trying to develop vanadium-free NH_3-SCR catalysts with high deNO_x efficiency, high N_2 selectivity, excellent hydrothermal stability and insensitivity to co-existing poisoning components in SCR atmosphere such as H_2O, SO_2, HC or alkali metals *etc*. Currently, metal oxide catalysts and zeolitic catalysts are two well-studied types of vanadium-free catalysts for the NH_3-SCR process in heavy-duty diesel engines, some of which show great potential in practical use [6, 9, 10]. However, despite the numerous studies on SCR performance under different conditions, a comprehensive summarization of the structure-activity relationship of these catalysts in the NH_3-SCR process is still lacking. In this article, taking Fe-, Ce-based oxide catalysts and Fe-, Cu-based zeolite catalysts as examples, we will discuss the microstructure of active sites, the role of acidity and also the activation of reactants on these catalysts for the NH_3-SCR reaction in detail, which is very important for the design of catalysts and study of reaction mechanisms.

On the other hand, since the pioneering work of Iwamoto *et al.* [11] and Held *et al.* [12], many catalysts such as zeolitic oxide, base oxide/metal and noble metal catalysts have been found to be effective for the SCR of NO_x with hydrocarbons (HC-SCR) in the presence of excess oxygen [3, 4, 7, 13-19]. Among the catalysts proposed for HC-SCR technology, zeolitic oxide catalysts are effective for NO_x reduction, while their water tolerance has been little improved [5]. Noble metal catalysts such as Pt/Al_2O_3 exhibit high deNO_x activity in the low temperature range of 200-300 °C

while exhibiting a narrow operation temperature window [20, 21]. Up to now, alumina-supported silver (Ag/Al_2O_3) has been known as one of the most effective catalysts for the HC-SCR even in the presence of water vapor and SO_2 [13, 16, 22-32]. The distinctive advantage of HC-SCR is that the on-board fuel can be used as the reductant for NO_x conversion, thus reducing the cost involved in infrastructure development for delivering reductant to the automotive engine exhaust system. The past several years have witnessed a growth in research in NO_x reduction by fuel-component hydrocarbons over Ag/Al_2O_3, while the light-off temperature for NO_x reduction is still too high to be used for commercial application in diesel vehicles, even though it has been reported that low temperature activity can be promoted by the addition of H_2 [24, 32-40]. More importantly, aromatic hydrocarbons, typically present in diesel fuel, give low activity for NO_x reduction even in the presence of H_2 [41]. Indeed, when using diesel fuel (ultra-low sulfur diesel, US06) as reductant [34], Ag/Al_2O_3 showed high initial activity for NO_x reduction in the presence of 3200 ppm H_2, while its activity gradually decayed with time, reaching a final conversion level similar to that observed in the absence of H_2. These results indicate that the issue of catalyst deactivation by hydrocarbon poisoning still needs to be resolved for the commercial application of HC-SCR. To provide a guideline for developing an ideal HC-SCR system, it is highly desirable to understand the mechanism of NO_x reduction by hydrocarbons at the molecular level.

2. Structure-activity relationship of vanadium-free catalysts for NH_3-SCR of NO_x

2.1. NH_3-SCR of NO_x over oxide catalysts

Many researchers have focused on the development of vanadium-free oxide catalysts for the NH_3-SCR process, which can be divided into single metal oxide catalysts, supported-type metal oxide catalysts and mixed metal oxide catalysts according to the forms of the catalytic materials. Based on the active components, the vanadium-free oxide catalysts can be further classified as Fe-, Ce-, Mn-, or Cu-based materials, of which the Fe- and Ce-based catalysts have been well studied in the deNO_x process of diesel engines due to their compatibility with the typical exhaust temperature range. In the following sections, we will systematically summarize the recent research advances in understanding the structure-activity relationship of Fe- and Ce-based oxide catalysts in the NH_3-SCR reaction, which are important for their practical use.

2.1.1. Fe-based oxide catalysts

Early in the 1980s, Kato *et al.* [42] used Fe_2O_3 as the active phase in a NH_3-SCR catalyst (*i.e.* Fe_2O_3-TiO_2 mixed oxide catalyst) with high SCR activity and N_2 selectivity at relatively high temperatures (350-450 ^oC), and thereafter numerous types of Fe_2O_3-containing catalysts were developed by researchers, including Fe_2O_3-pillared layered clay (PILC) [43], Fe_2O_3-SiO_2 [44], Fe_2O_3 supported on activated carbon (AC) [45] or activated carbon fiber (ACF) [46] *etc.* Yet at that time, no systematic studies of the microstructure of Fe species and its relationship with SCR performance were reported.

Several years ago, Apostolescu *et al.* [47] developed a new supported-type $Fe_2O_3/WO_3/ZrO_2$ catalyst achieving total NO_x conversion and high N_2 selectivity in the NH_3-SCR reaction over the temperature range 280-430 ^oC. Based on a series of characterization results including XRD and H_2-TPR, they pointed out that the Fe species in the $Fe_2O_3/WO_3/ZrO_2$ catalyst were mainly present in the form of well-crystallized Fe_2O_3 and also small Fe_xO_y particles. During the NH_3-SCR reaction, the Fe^{3+} species catalyzed the dehydrogenation of NH_3 to NH_2 while being reduced to Fe^{2+} species, and thereafter the NH_2 species reacted with gaseous NO to produce N_2 and H_2O, while O_2 could re-oxidize Fe^{2+} species to Fe^{3+} species participating into the next redox cycle. The SCR reaction over this catalyst mainly followed an Eley-Rideal (E-R) mechanism. This is probably the first successful example elucidating the structure-activity relationship of Fe species in the NH_3-SCR reaction for an Fe_2O_3-containing oxide catalyst.

Usually, it is also accepted that NO can be molecularly adsorbed on the transition metal ion or it can dissociatively chemisorb on oxide ion vacancies of the metal oxide catalysts, and react with adsorbed NH_3 or NH_4^+ species to form SCR reaction intermediates and decompose into N_2 and H_2O afterwards, following a Langmuir-Hinshelwood (L-H) mechanism. To effectively disperse the active species, anatase TiO_2 is usually utilized as the catalyst support for the NH_3-SCR reaction. Although it is inert for NO_x conversion, its acidity can inhibit the formation of sulfate species on the catalyst surface in SO_2-containing atmospheres above 200 ^oC to avoid the deactivation of SCR catalysts [48]. Based on the above-mentioned ideas, Roy *et al.* [49] prepared an Fe ion substituted TiO_2, namely the $Ti_{0.9}Fe_{0.1}O_{2-\delta}$ catalyst, by a novel single-step solution combustion method, showing total NO_x conversion at *ca.* 300-425 ^oC with rather high N_2 selectivity. Compared with the well-crystallized ilmenite phase $FeTiO_3$ over which the maximum NO_x conversion did not exceed 20%, the catalytic activity of the $Ti_{0.9}Fe_{0.1}O_{2-\delta}$ catalyst with ionic metal sites and oxide ion vacancies was much higher, indicating that such defect structures in NH_3-SCR catalysts were important factors influencing their catalytic performance in the deNO_x process.

Over the $Ti_{0.9}Fe_{0.1}O_{2-\delta}$ catalyst, Roy *et al.* [49] considered that the Lewis acid sites were beneficial to the wide SCR operation temperature window, and for the $Fe_2O_3/WO_3/ZrO_2$ catalyst prepared by Apostolescu *et al.* [47], the importance of Lewis acid sites to the E-R mechanism of the NH_3-SCR reaction was also strongly emphasized. However, for the supported-type $Fe_2(SO_4)_3/TiO_2$ catalyst prepared by Ma *et al.* [50] with high NO_x conversion at 350-450 ^oC, they considered that the relatively strong Brønsted acid sites induced by sulfate species contributed substantially to the deNO_x efficiency. Thus, the roles of Lewis acid sites and Brønsted acid sites in the NH_3-SCR reaction over Fe_2O_3-containing catalysts are still in debate, and in future study, we strongly recommend that the elucidation of the involvement of these two types of acid sites in the NH_3-SCR reaction should be closely correlated to the reaction temperature.

In recent years, we have focused on the investigation of the structure-activity relationship of iron titanate ($FeTiO_x$) catalysts in the NH_3-SCR reaction. This environmentally-friendly catalyst, when prepared by a co-precipitation method using $Fe(NO_3)_3$ and $Ti(SO_4)_2$ as precursors, showed high SCR activity, N_2 selectivity

and H_2O/SO_2 durability in the medium temperature range (200-400 °C) [51], and an operation temperature window at least 50-150 °C lower than those of the above-mentioned Fe_2O_3-containing catalysts. Compared with the $FeTiO_x$ catalyst prepared using $TiCl_4$ as precursor and Fe_2O_3/TiO_2 catalyst prepared by an impregnation method, the existence of sulfate species in the preparation process could significantly inhibit the crystallization of mixed metal oxide phases, resulting in the formation of highly dispersed small iron titanate crystallites, which is totally different from the Fe_2O_3 particles normally found in previously reported studies [52]. A similar promotion effect by sulfate species on the dispersion of Fe species was also observed by Ma *et al.* on their $Fe_2(SO_4)_3/TiO_2$ catalyst [50]. Thereafter, the microstructure of iron titanate crystallites in $FeTiO_x$ catalysts was studied in detail using various characterization methods, including N_2 physisorption, Powder XRD, UV-vis DRS, Raman spectroscopy and XAFS *etc*., and the surface chemical composition and redox behavior were studied using XPS and H_2-TPR. It was definitively concluded that the active iron titanate crystallites in the $FeTiO_x$ catalyst prepared at low calcination temperature were mainly in the form of a specific edge-shared Fe^{3+}-$(O)_2$-Ti^{4+} structure (Scheme 1), and had large surface area, pore volume and abundant surface defects supplying rich catalytically active sites for the NH_3-SCR reaction. In this specific edge-shared Fe^{3+}-$(O)_2$-Ti^{4+} structure, the existence of an electronic inductive effect between Fe^{3+} species and Ti^{4+} species was confirmed, leading to higher NO adsorption and oxidation ability for Fe^{3+} species and thus higher SCR activity at low temperatures [52, 53]. Although after high temperature calcination such as at 600 or 700 °C, the specific surface area and reactant adsorption ability of the $FeTiO_x$ catalyst was decreased to a certain extent due to the occurrence of sintering (*i.e.* well-crystallized Fe_2TiO_5 was formed), the intrinsic SCR activity normalized by surface area was actually increased [54]. In future study, the deposition of such iron titanate crystallites onto microporous or mesoporous materials with large surface area holds promise as a method to enhance its dispersion and thermal stability for practical utilization in industry.

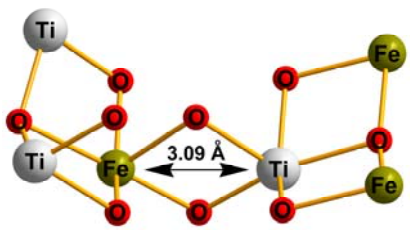

Scheme 1. Proposed model of homogeneous edge-shared Fe^{3+}-$(O)_2$-Ti^{4+} structure in $FeTiO_x$ catalyst (Reproduced with permission from Elsevier Inc.) [53]

Using *in situ* DRIFTS, transient response experiments and temperature programmed desorption/surface reaction methods, the NH_3-SCR reaction mechanism over the $FeTiO_x$ catalyst was well studied (Scheme 2) [55]. At temperatures below 200 °C, on the Fe^{3+}-$(O)_2$-Ti^{4+} structure, NO can be oxidized into nitrate species on Fe^{3+} sites and then react with adjacent adsorbed NH_3 species on Ti^{4+}-OH Brønsted acid sites to form intermediate species (similar to ammonium nitrate species), followed by subsequent reaction with gaseous NO to produce N_2 and H_2O. An L-H mechanism is proposed accordingly for NH_3-SCR of NO_x at low temperatures over the $FeTiO_x$ catalyst, in which the formation of reactive monodentate nitrate on Fe^{3+} sites is the rate-determining step [55]. An efficient method to improve the low temperature SCR activity of the $FeTiO_x$ catalyst is to enhance the NO_x adsorption as monodentate nitrate [56], as confirmed by subsequent experimental results in which the low temperature SCR activity was greatly enhanced through partial substitution of Fe species by Mn species in $FeTiO_x$ with considerably enhanced formation of monodentate nitrates [57]. If SO_2 is present in the NH_3-SCR atmosphere, the sulfate species will preferentially adsorb onto Fe sites to form Fe-O-S bonds (as evidenced by EXAFS results) competing with the adsorption of nitrate species, leading to the decline of low temperature SCR activity to a certain extent [58]. This inhibition effect is more prominent on Mn-substituted $FeTiO_x$ catalysts, mainly due to the easier blocking of the L-H reaction pathway at low temperatures by sulfate deposition on Mn sites [59]. In future study, the simultaneous improvement of the low temperature SCR activity and SO_2 durability of Fe-containing catalysts is still a great challenge, unless a completely new reaction pathway different from L-H mechanism can be opened by catalyst modification or redesign.

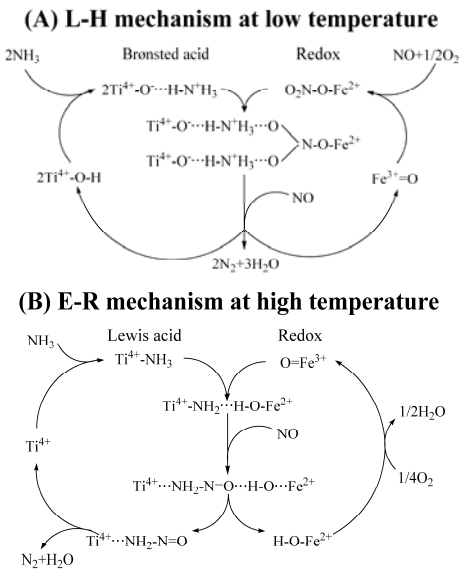

Scheme 2. Proposed SCR mechanisms over $FeTiO_x$ catalyst in different temperature ranges (Reproduced with permission from Elsevier Inc.) [55]

Returning to the $FeTiO_x$ catalyst, at temperatures above 200 °C, the Ti^{4+}-OH Brønsted acid sites can be transformed into Lewis acid sites through dehydroxylation, and then adsorb NH_3 to participate in the NO_x reduction process. The adsorbed NH_3 species can be activated into -NH_2 species by neighboring Fe^{3+} sites through dehydrogenation, and thereafter react with gaseous NO to form a NH_2NO intermediate and decompose into N_2 and H_2O. In this process, the Fe^{3+} species is first reduced to Fe^{2+} species and then reoxidized to Fe^{3+} species by gaseous O_2, completing a redox cycle. A typical E-R mechanism for NH_3-SCR of NO_x at high temperatures over the $FeTiO_x$ catalyst is proposed accordingly, with the formation of NH_2NO being the rate-determining step [55]. Although sulfate species may also form on Fe^{3+} sites in this process, the activation of NH_3 to -NH_2 species is not influenced. Therefore, the E-R reaction pathway

can still proceed over the sulfated $FeTiO_x$ catalyst, ensuring high $deNO_x$ efficiency at relatively high temperatures [58]. In brief, this was possibly the first time that different NH_3-SCR mechanisms over Fe-containing catalysts in the low and high temperature ranges with the involvement of both acid sites and redox sites was demonstrated. Since then, researchers have started to pay attention to the influence of reaction temperature on the NH_3-SCR mechanism over different types of catalysts, such as the Fe-Ti spinel catalyst [60], CeO_2/TiO_2, CeO_2-WO_3/TiO_2 catalysts [61] and CuO_x/WO_x-ZrO_2 catalyst [62] *etc*. In future study, the hydrothermal stability and resistance to coexisting poisoning pollutants in the SCR atmosphere (*i.e.* H_2O, SO_2, HC, alkali metals *etc.*) of this $FeTiO_x$ catalyst still need to be investigated in more detail before its practical use in $deNO_x$ process of diesel engines.

The above-mentioned Fe-containing catalysts are usually in the form of supported-type or mixed oxides, with the second or third component acting as support or promoter. Actually, the well-designed Fe_2O_3 oxide itself can also show good performance in the NH_3-SCR reaction, and this type of material has obvious advantages for the investigation of the structure-activity relationship. Very recently, the synthesis of Fe_2O_3 nanomaterials with controlled crystal phase and morphology has achieved great success [63]. Over α-Fe_2O_3 samples prepared by Yang *et al.* [64] by a hydrothermal route with nanocube and nanorod morphologies, the relationship between NH_3-SCR activity and exposed crystal facet was established. They concluded that α-Fe_2O_3 nanorods exposing more (110) facets with relatively higher surface energy and higher density of Fe atoms showed much better NH_3-SCR activity than α-Fe_2O_3 nanocubes mainly exposing (012) facets with low surface energy. Mou *et al.* [65] creatively synthesized novel α-Fe_2O_3 nanorods and γ-Fe_2O_3 nanorods by aqueous precipitation and calcination/refluxing methods, showing the same morphology but totally different exposed crystal facets. They clearly concluded that the γ-Fe_2O_3 nanorods enclosed by reactive (110) and (100) facets, simultaneously exposing Fe^{3+} and O^{2-} sites, were highly active for the activation of NH_3 and NO, and thus highly active for the NH_3-SCR reaction. In contrast, the α-Fe_2O_3 nanorods enclosed by (210) and (001) facets only exposed Fe^{3+} sites and showed relatively poor SCR activity, due to the lack of neighboring oxygen anions for the activation of NH_3 and NO. These studies have significantly elevated the research on the structure-activity relationship of Fe_2O_3 catalysts for the NH_3-SCR reaction to a new height, and in the near future studies on their practical utilization should be more focused.

2.1.2. Ce-based oxide catalysts

In previous studies, cerium oxide has usually been employed as the promoter or support for NH_3-SCR catalysts. For example, Chen *et al.* [66] added *ca.* 10 wt.% Ce to a V_2O_5-WO_3/TiO_2 catalyst with low vanadia loading (0.1 wt.%), which was able to greatly improve the NH_3-SCR activity in a broad operation temperature window. Long and Yang [67] found that Ce doping could enhance the stability of Fe-ZSM-5 catalysts, and Carja *et al.* [68] concluded that the synergistic effect between Fe and Ce in Fe-Ce-ZSM-5 catalysts could greatly improve the $deNO_x$ efficiency. Wu *et al.* [69, 70] concluded that a Ce-promoted Mn/TiO_2 catalyst showed better SO_2 resistance in the low temperature NH_3-SCR process. Li *et al.* [71] prepared a supported WO_3 catalyst using CeO_2-ZrO_2 mixed oxide as support, exhibiting excellent NH_3-SCR activity and thermal stability, as a potential candidate for the $deNO_x$ process of diesel engines.

With the increase of understanding on the effect of cerium oxide in the NH_3-SCR reaction, researchers have begun to realize that this material with excellent redox properties can also be used as an active component in SCR catalysts. For instance, Xu *et al.* [72] reported a novel Ce/TiO_2 catalyst, prepared by a conventional precipitation method, showing high $deNO_x$ efficiency and N_2 selectivity from 250 to 400 °C. Afterwards, Gao *et al.* [73, 74] investigated the influence of preparation methods (including sol-gel, impregnation and co-precipitation methods) and concluded that the catalyst prepared by the sol-gel method showed the best catalytic performance. They considered that the relatively strong interaction between Ce and Ti species and also the high dispersion of CeO_2 crystallites on the TiO_2 surface were important for the NH_3-SCR reaction. Although the SCR activity of the Ce/TiO_2 catalyst has been proved to be outstanding, the resistance to SO_2 poisoning and high space velocity (GHSV) still need to be enhanced for practical use. For example, the supported Ce/TiO_2 catalyst can be deactivated by SO_2 through the formation of highly thermally stable $Ce(SO_4)_2$ and $Ce_2(SO_4)_3$, cutting off the redox cycle between Ce^{3+} and Ce^{4+} species [75]. In addition, with increasing GHSV, the insufficient SCR activity, especially at low temperatures, cannot satisfy the requirements for practical use in diesel engines [72, 73]. To overcome these shortcomings, Shan *et al.* [76] simply developed a homogeneous precipitation method characterized by uniform increase of pH value through decomposition of an organic base (urea in this study) to prepare a $CeTiO_x$ mixed oxide catalyst. During this process, the TiO_x species was first precipitated at the initial stage and afterwards the CeO_x species was precipitated uniformly onto the TiO_x species, forming many catalytically active $CeTiO_x$ crystallites [77]. This $CeTiO_x$ catalyst showed much higher SCR activity than the supported Ce/TiO_2 catalyst (Fig. 1), with significantly improved resistance to high space velocity.

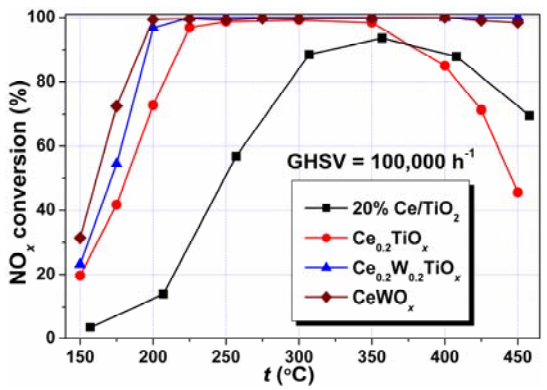

Fig. 1. NH_3-SCR activity over 20% Ce/TiO_2, $Ce_{0.2}TiO_x$, $Ce_{0.2}W_{0.2}TiO_x$, $CeWO_x$ catalysts in simulated diesel engine exhaust

To better enhance the catalytic performance together with the thermal stability of this $CeTiO_x$ catalyst, doping with W species was carried out (Fig. 1) [78]. Over the optimal $Ce_{0.2}W_{0.2}TiO_x$ catalyst with Ce:W molar ratio of 1:1, NO_x conversion could be maintained above 90% from 275 to 450 °C even under the rather high GHSV of 500,000 h^{-1}. The W doping in the $Ce_{0.2}W_{0.2}TiO_x$

catalyst led to a much higher dispersion degree of Ce species, with a larger Ce^{3+}/Ce^{4+} ratio and more oxygen vacancies, resulting in higher NO oxidation ability and thus better SCR activity at low temperatures. In addition, due to the increased capacity for adsorption of NH_3 species on both Brønsted acid sites and Lewis acid sites induced by W doping, the NH_3 unselective oxidation at high temperatures was also greatly inhibited, thus leading to higher SCR activity and N_2 selectivity simultaneously. A similar promotion effect by W species on CeO_2/TiO_2 supported-type catalysts was also observed by Chen *et al.* [79], which they attributed to the strong interaction between Ce and W species.

Actually, for TiO_2-containing NH_3-SCR catalysts, the activity loss at high temperatures above 600 °C is usually associated with the occurrence of a phase transformation from anatase to rutile. Through analysis of the effect of W species in the $Ce_{0.2}W_{0.2}TiO_x$ catalyst, Shan *et al.* [80] had the idea to substitute all Ti species by W species. Under this inspiration, a novel and excellent $CeWO_x$ catalyst with high NH_3-SCR activity, outstanding N_2 selectivity, improved thermal stability, good durability toward co-existing pollutants and especially much higher resistance to space velocity was developed (Fig. 1). Even under the very high GHSV of 500,000 h^{-1}, the NO_x conversion over $CeWO_x$ could also be maintained at 100% from 250 to 425 °C, which is very beneficial for practical use in diesel vehicles with limited installation space for SCR converters. Based on various characterization results, it was concluded that, compared with pristine oxides, the strong interaction between Ce and W species led to higher dispersion of CeO_2 and WO_3 crystallites and more abundant Ce^{3+} species with higher concentration of surface oxygen species, which were important for the oxidation of NO, thus promoting the "fast SCR" reaction. The synergistic effect between Ce and W species produced more Brønsted acid sites and Lewis acid sites for NH_3 adsorption and also maintained enough capacity for NO_x adsorption, achieving a broad operation temperature window in the NH_3-SCR reaction. This $CeWO_x$ catalyst is a fascinating candidate for the $deNO_x$ process from diesel engines, and Chen *et al.* [81] also found this advantageous combination of Ce and W species in a CeO_2-WO_3 mixed oxide catalyst at nearly the same time. Peng *et al.* [82, 83] found that this catalyst could resist greater amounts of alkali metals than V_2O_5-WO_3/TiO_2 and that Mn doping could further improve its low temperature SCR activity. Over this CeO_2-WO_3 mixed oxide catalyst, based on an *in situ* DRIFTS study, Chen *et al.* [84] proposed two reaction pathways of NH_3-SCR reaction which were similar to the E-R and L-H mechanisms. However, much more work needs to be done to better understand the intrinsic SCR reaction mechanism over this novel material, especially using other characterization methods.

Besides the above-mentioned materials, CeO_2 supported on Al_2O_3 [85], activated carbon fibers [86], and carbon nanotubes [87] together with a hydrothermally synthesized Ce-P-O catalyst [88], were also developed by other researchers, all showing impressive $deNO_x$ efficiency, although the detailed structure-activity relationship of these CeO_2-containing catalysts in NH_3-SCR reaction still needs to be studied. In the aspect of catalyst structure design, Wang *et al.* [89] developed a novel titanium nanotube-confined CeO_2 catalyst, showing higher NH_3-SCR activity than that of CeO_2 supported on TiO_2 nanoparticles, mainly due to the possession of stronger redox ability and NH_3 adsorption capacity, judging from comparison of the H_2-TPR and NH_3-TPD results, respectively. Owing to the presence of a "shell protection effect", Chen *et al.* [90] found that this titanium-nanotube-confined CeO_2 catalyst showed a remarkable resistance to alkali metal poisoning in the $deNO_x$ process. This result provides a new route for synthesis of NH_3-SCR catalysts with higher poisoning resistance for practical use. Recently, the surface modification of CeO_2 by WO_x [91] or sulfate species [92] and the surface modification of CeO_2-ZrO_2 solid solutions by nickel/sulfate species [93] or phosphate species [94] to promote the NH_3-SCR activity also achieved some progress, in which the roles of acid sites induced by surface modifiers and the inhibition of NH_3 un-selective oxidation at high temperatures were carefully addressed. In future study, the surface modification of CeO_2 or other metal oxides could be a promising way to prepare applicable catalysts that is also convenient for studying their structure-activity relationships in the NH_3-SCR reaction.

2.2. NH_3-SCR of NO_x over zeolite catalysts

Zeolite catalysts have received much attention in recent years due to their excellent SCR activity and thermal stability for the $deNO_x$ process in diesel engines [3]. Owing to the complexity of zeolite structures (*e.g.* ZSM-5, HBEA, MOR, USY, CHA *etc.*), the difference in preparation methods (*e.g.* aqueous ion-exchange, solid-state ion-exchange, incipient wetness impregnation, chemical vapor deposition, one-pot synthesis *etc.*) together with the differences in active metal sites (*e.g.* Fe, Cu *etc.*), a universally accepted structure-activity relationship for zeolite catalysts in the NH_3-SCR reaction cannot be easily established. Fortunately, many researchers have devoted themselves to relatively fundamental research on zeolite NH_3-SCR catalysts besides work aimed toward their industrially practical use. The enlightening results obtained in this area will be introduced in the following sections classified by the Fe and Cu transition metals commonly used as active sites.

2.2.1. Fe-based zeolite catalysts

Among the numerous Fe-based zeolite catalysts, the application of Fe-ZSM-5 in the NH_3-SCR reaction has attracted much attention from researchers since the end of the last century. In 1999, Ma and Grünert [95] and Long and Yang [67] both reported that Fe-ZSM-5 catalysts prepared by over-exchange of Fe into H-ZSM-5 through $FeCl_3$ sublimation and ion-exchange of Fe into NH_4-ZSM-5 using $FeCl_2$ as precursor, respectively, showed excellent NH_3-SCR activity even under high GHSV and in the presence of SO_2. Thereafter, more and more researchers focused on the study of Fe-ZSM-5 catalysts, investigating the influence of preparation methods, Fe exchange level and Si/Al ratio *etc.* on NH_3-SCR activity [10].

Although different research groups reported diverse optimal methods for preparation of Fe-ZSM-5 catalysts with high apparent SCR activity, such as the improved aqueous ion-exchange method by Long and Yang [96], the solid-state ion exchange method by Schwidder *et al.* [97], and the chemical vapor deposition method by Iwasaki *et al.* [98], the researchers eventually concluded that the preparation method was actually not a decisive factor in determining the intrinsic catalytic activity

of Fe-ZSM-5 catalysts in the NH_3-SCR reaction (*i.e.* the turnover frequency), but the microstructure of Fe species was [10, 98]. Brandenberger *et al.* [99] recently systematically studied the different Fe sites located in Fe-ZSM-5 catalysts including monomeric, dimeric, clustered and oligomeric species, and correlated them with the measured NH_3-SCR activity (Scheme 3). They concluded that actually all Fe species in the Fe-ZSM-5 catalyst were active, although they exhibited different temperature dependencies in the SCR reaction. Below 300 °C, only monomeric Fe species contributed to the SCR reaction, and this type of Fe species did not catalyze the NH_3 unselective oxidation below 500 °C, which was beneficial to high N_2 selectivity. The important role of monomeric Fe^{3+} sites was also emphasized by Høj *et al.* [100] in their Fe-BEA catalyst. Above 300, 400 and 500 °C, respectively, the dimeric Fe species, the oligomeric species (*e.g.* trimeric and tetrameric Fe species) and partially uncoordinated Fe sites in the outmost layer of Fe_xO_y particles could also contribute to the NH_3-SCR reaction, and at high temperatures (> 500 °C) the contribution of dimeric Fe species dominated. However, the unselective oxidation of NH_3 would occur on Fe_xO_y particles above 350 °C, resulting in low N_2 selectivity, and the dimeric Fe species governed the NH_3 oxidation up to 500 °C. A similar effect by severely clustered Fe_xO_y species on the unselective consumption of the reducing agent NH_3 in the SCR reaction was also proposed by Schwidder *et al.* [101] and Devadas *et al.* [102]. Therefore, to obtain excellent NH_3-SCR activity at low temperatures together with good N_2 selectivity at high temperatures, an Fe-zeolite catalyst with a maximum quantity of monomeric Fe^{3+} sites should be prepared. Although some other factors may also influence the apparent SCR activity of Fe-zeolite catalysts [103], the conclusions drawn by Brandenberger *et al.* [99] in the above-mentioned study are generally useful for the design, synthesis and application of efficient Fe-zeolite catalysts.

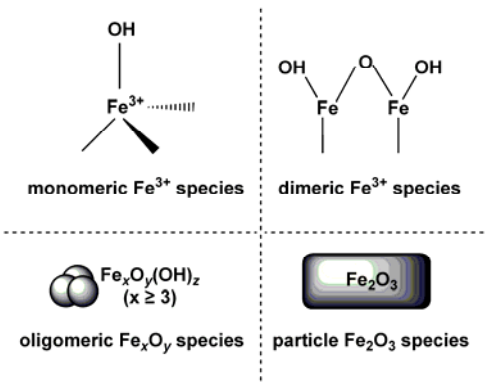

Scheme 3. The Fe species probably present in Fe-zeolite NH_3-SCR catalysts

Besides the nature and effect of Fe species in Fe-zeolite catalysts, researchers also have paid close attention to the influence of the acidic properties of zeolite materials on the NH_3-SCR reaction. On Fe-based zeolite catalysts with the same type of framework structure, the SCR activity usually increases with decreasing Si/Al ratio [104, 105], although the hydrothermal stability of zeolites deteriorates to a certain extent. Early work simply considered that the increase of SCR activity with low Si/Al ratio corresponded to the enhancement of Brønsted acidity induced by aluminium sites (Al-OH) [106], and that the NH_4^+ species adsorbed on Brønsted acid sites directly participated in the SCR reaction to reduce NO_x [107]. However, after extensive study, the researchers finally realize that the Brønsted acidic property is actually not a decisive factor for the high NH_3-SCR activity of Fe-zeolite catalysts, because over some zeolite materials without acidic sites, high NO_x conversion rates could still be obtained [108]. Yet, in another aspect, a promotion effect by Brønsted acidity on the NH_3-SCR reaction could still be observed if the catalysts contained the most favorable Fe species, and Schwidder *et al.* [108] concluded that this was probably due to the obvious promotion of an acid-catalyzed intermediate step in the NH_3-SCR reaction (*e.g.* the decomposition of NH_4NO_2) similar to the results reported by Li *et al.* [109] and Savara *et al.* [110], which might be the rate-determining step at low temperatures. In addition, Brandenberger *et al.* [111] concluded that the Brønsted acid sites might not be required directly in the SCR process for adsorbing or activating NH_3, but they were necessary to bind and disperse the reactive Fe^{3+} ions in the preparation process for Fe-based zeolite catalysts, similar to the results reported by Iwasaki *et al.* [104]. Furthermore, the zeolite support with Brønsted acidity could also play a role as NH_3 reservoir, regardless of the form in which the NH_3 was stored, and in the NH_3-SCR reaction the stored NH_3 could migrate to the active sites so as to undergo a reaction with NO [111]. A similar spill-over effect of NH_3 on the zeolite support to the active Fe^{3+} sites in the NH_3-SCR reaction was also reported by Klukowski *et al.* [112] on their Fe-HBEA catalyst. Therefore, in brief summary, nowadays researchers basically agree that in the standard NH_3-SCR reaction the oxidation function of Fe-based zeolite catalysts and the amount of active Fe species, but not the acidic properties of the zeolite supports, are the main factors controlling the deNO_x efficiency [104, 111].

Hydrothermal stability is an important factor for the practical use of Fe-based zeolite catalysts, to which the researchers also paid great attention. Hydrothermal treatment could result in the dealumination of zeolite supports, leading to the decrease of Brønsted acid sites or breakdown of the framework structure, and more seriously the migration of active Fe^{3+} species to form clustered Fe_xO_y/Fe_2O_3 species, leading to the decline of NH_3-SCR activity and N_2 selectivity [113-116]. The remaining NH_3-SCR activity after hydrothermal aging at different conditions was mainly attributed to the residual monomeric Fe^{3+} species located at ion exchange sites [114]. The use of zeolite supports with high Si/Al ratio is expected to result in acceptable hydrothermal stability, but the SCR activity may be negatively affected owing to the presence of fewer Brønsted acid sites to exchange, bind and disperse active Fe^{3+} sites. Recently, Iwasaki and Shinjoh [117] successfully improved the hydrothermal stability of Fe-BEA catalysts by sequential ion-exchange of rare earth (RE) metals, and concluded that the improvement was dependent on the ionic radius of the exchanged metals. When using the RE metals with radii of 1.05-1.15 Å such as Ce, Nd, Sm, Gd and Tb, the dealumination of aged Fe-BEA catalyst was clearly reduced. This method could also be useful with other Fe-based zeolite catalysts for the effective improvement of hydrothermal stability in practical use.

Another important deactivation factor for Fe-based zeolite catalysts is hydrocarbon (HC) poisoning, which is closely related

to the dimensional structure of zeolite supports. For example, on Fe-ZSM-5 and Fe-BEA catalysts with three-dimensional structure, after HC poisoning the NH_3-SCR activity, especially at low temperatures, was markedly decreased mainly due to carbonaceous deposition. This resulted in the decline of surface area and pore volume together with suppressed NO oxidation ability for blocked Fe^{3+} sites, or the partial reduction of Fe^{3+} species to Fe^{2+} by HC, or the competitive adsorption of HC with NH_3/NO onto the catalyst surface [113, 118, 119]. The deactivation effect of HC on NH_3-SCR activity was less on the Fe-MOR catalyst with one-dimensional structure due to the difficulty in HC diffusion, and using this feature Ma *et al.* [120] effectively improved the HC resistance of a modified Fe-BEA monolith catalyst by coating another layer of MOR zeolite on the outer surface. This useful modification strategy is worthy of application in the preparation of other efficient NH_3-SCR monolith catalysts for the control of emissions from diesel engines.

In practical use, the low temperature NH_3-SCR activity of Fe-based zeolite catalysts still needs improvement to meet the diesel emission standards for cold-start and idle speed processes [121], especially in the regions where Cu-based zeolite catalysts cannot be used, such as in Japan [122]. The relevant methods include the addition of catalyst promoters such as RE metal Ce [68] and noble metal Pt [123], together with the tuning of the reaction atmosphere, such as raising the NO_2 ratio in NO_x to facilitate the "fast SCR" reaction [124, 125] and adding a small amount of NH_4NO_3 solution as an effective oxidant for NO, creating a similar "fast SCR" reaction condition [126]. In addition, to enable practical utilization of the catalysts, the deactivation effects of inorganic components contained in diesel exhaust on Fe-based zeolite catalysts are also worthy of investigation, including the combustion products of lubricant oil additives (*i.e.* Ca, Mg, Zn, P, B, Mo), the impurities of biodiesel fuel/urea solution (*i.e.* K, Ca) together with the aerosol particulates from intake air (*i.e.* Na, Cl) [127]; these issues will not be discussed in detail due to the length limit of this article.

2.2.2. Cu-based zeolite catalysts

Since the zeolite catalysts began being used in the NH_3-SCR reaction in the late 1970s, the Cu-based zeolite catalysts (mainly Cu-exchanged Y zeolites) have shown relatively good catalytic performance among the studied materials [5]. In the 1990s, the Cu-based zeolite catalysts attracted more attention from researchers in the field of catalytic deNO_x from diesel engine exhaust. Cu-ZSM-5 catalysts have been well studied in early works, and showed excellent low temperature NH_3-SCR activity and broad operation temperature window even using urea as reductant [128]. Sjövall *et al.* [129] concluded that using a zeolite support with low Si/Al ratio and increasing the Cu loading could noticeably enhance the NH_3-SCR activity of Cu-ZSM-5 catalysts. Qi *et al.* [105] reported that Cu-ZSM-5 catalysts showed high deNO_x performance at medium and low temperatures even under high GHSV, but the hydrothermal treatment could result in a decline in activity to a certain extent.

Actually, comparative studies showed that the preparation method, the Cu loading and even the precursors used for ZSM-5 synthesis could influence the hydrothermal stability of Cu-ZSM-5 catalysts [105, 128, 130]. It is generally accepted that the active sites in the SCR reaction of Cu-based zeolites, including Cu-ZSM-5, Cu-beta and Cu-FAU, are mainly dimerized Cu^{2+} and Cu^{+} species, and the facility of redox between Cu^{2+} and Cu^{+} is beneficial to high SCR performance [10, 128, 131-135]. Through studies on the variation of SCR activity and the alteration of catalytically active sites, Park *et al.* [131] attributed the hydrothermal deactivation of Cu-ZSM-5 catalysts to the migration and re-distribution of Cu^{2+} species, leading to the decrease of active sites and the blockage of zeolite channels by sintered CuO, together with the dealumination and collapse of the zeolite support. After hydrothermal treatment of Cu-beta catalysts under different conditions (500-90 ^{o}C, 3% H_2O), Wilken *et al.* [134] found that the zeolite structure showed no obvious change below 800 ^{o}C, yet the oxidation state of Cu species showed apparent change, with a decrease in Cu^{+} species and increase in Cu^{2+} species as indicated by XPS results. Peden *et al.* [135] found that after severe hydrothermal treatment of Cu-beta catalysts at 900 ^{o}C for 2 h with 2% H_2O, the zeolite structure showed clear collapse. Therefore, in brief, the main reasons for the hydrothermal deactivation of Cu-based zeolite catalyst are the instability of active Cu species and of zeolite structures. Interestingly, Moden *et al.* [136] reported that the active Cu species in Cu-FER catalysts with smaller pore size (0.42 × 0.54 nm) showed higher hydrothermal stability than that in Cu-beta catalysts with relatively larger pore size (0.66 × 0.67 nm). Nanba *et al.* [137-139] also observed that in the presence of *n*-decane, NO_x conversion in the NH_3-SCR reaction over the Cu-FER catalyst was less affected than that over Cu-ZSM-5. Thus, it is expected that using a zeolite support with smaller pore size may produce Cu-based zeolite catalysts with exceptional NH_3-SCR activity, outstanding hydrothermal stability and HC resistance simultaneously.

Recently, Kwak *et al.* [140, 141] and Fickel *et al.* [142] reported a series of Cu-chabazite (Cu-CHA) catalysts including Cu-SSZ-13 and Cu-SAPO-34, showing high NH_3-SCR activity, good N_2 selectivity and excellent hydrothermal stability with great application potential in the deNO_x process of diesel engines. Fickel *et al.* [142] considered that the excellent hydrothermal stability of Cu-SSZ-13 and Cu-SAPO-34 catalysts was mainly due to the unique structure of CHA zeolites containing eight-membered-ring pores with small pore size (0.38 × 0.38 nm). For example, the ^{27}Al-NMR results by Kwak *et al.* [140] showed that the hydrothermally treated Cu-SSZ-13 catalyst showed no noticeable change in the peak intensity of AlO_4 species compared with the fresh catalyst; however, the peak intensity of AlO_4 species in Cu-ZSM-5 and Cu-beta catalysts decreased *ca.* 57% and 31%, respectively, suggesting an obvious dealumination process. Based on the commercial Cu-CHA catalyst from BASF Corporation, Schmieg *et al.* [143] found that even after hydrothermal treatment at 800 ^{o}C for 16 h, which was comparable to 135,000 mile vehicle-ageing, this catalyst still exhibited more than 70% NO_x conversion from 200 to 450 ^{o}C. The small pore structure in Cu-CHA catalysts was also expected to be more resistant to HC poisoning due to the difficulty in diffusion of HC with larger size, such as isobutane, with a kinetic diameter of 5.5 Å [142].

Using a variable-temperature XRD method, Fickel and Lobo [144] proved that the ion-exchange of Cu species into NH_4-SSZ-13 could greatly enhance its thermal stability. Through a

comprehensive study using Rietveld refinement of the XRD data, *in situ* UV-Vis and XAFS techniques, Fickel and Lobo [144], Korhonen *et al.* [145] and Deka *et al.* [146] finally concluded that only the isolated Cu^{2+} species located in the six-membered-rings of CHA structure coordinating with three oxygen atoms was the real active species in the NH_3-SCR reaction (Scheme 4). Using *operando* XAFS, density functional theory (DFT) calculation, and first-principles thermodynamics models, Kispersky *et al.* [147] and McEwen *et al.* [148] proposed that under the standard NH_3-SCR conditions at steady state, the active Cu species was actually in a mixture of Cu^+ species and Cu^{2+} species, indicating that the redox cycle between Cu^+/Cu^{2+} is very important for high NH_3-SCR activity, similar to other Cu-based zeolite catalysts. Very recently, a further study using H_2-TPR and FTIR methods by Kwak *et al.* [149] revealed two distinct cationic positions in Cu-SSZ-13 catalysts at different ion-exchange levels. They concluded that at low ion-exchange levels, the Cu^{2+} ions primarily occupied the sites in the six-membered-rings similar to those identified in early reports, while at high ion-exchange levels, the Cu^{2+} ions were present mostly in the large cages of the CHA structure. The latter Cu^{2+} species were much more easily reduced in the H_2-TPR process, indicating a high redox capability at low temperatures, which might be the main origin of the exceptional NH_3-SCR activity over Cu-SSZ-13 catalysts. Therefore, although the NH_3-SCR performance of Cu-CHA catalysts has been well recognized, the understanding of the intrinsic active Cu sites is still in debate and ongoing. Besides, Kwak *et al.* [150] noticed that regardless of Cu ion-exchange degree, the NO oxidation ability of Cu-SSZ-13 catalysts was very low; even under the "fast SCR" condition, the NO_x conversion was only slightly improved, with little formation of N_2O. Compared with other Cu-based zeolite catalysts or even other NH_3-SCR catalysts, the above-mentioned "abnormal" results indicate that a totally different NH_3-SCR reaction mechanism may exist over the Cu-SSZ-13 catalyst, which needs be investigated in detail using various methods in future research. In addition, new types of Cu-based zeolite catalysts are being developed constantly with high deNO_x efficiency, such as the newly reported Cu-SSZ-39 with AEI structure, which also shows extraordinary hydrothermal stability [151]. Consequently, study of the structure-activity relationship of Cu-based zeolite catalysts in the NH_3-SCR reaction will always be a hotspot in the field of environmental catalysis.

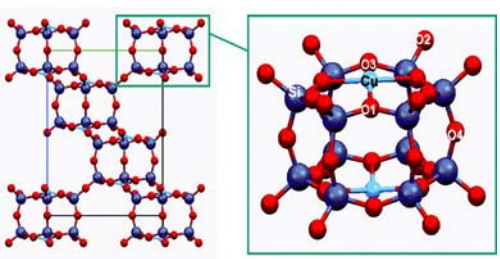

Scheme 4. The structure of Cu-SSZ-13 obtained from refinements of neutron scattering data, and magnification of the double six member (d6r) unit with Cu present as an isolated ion (Reproduced with permission from American Chemical Society) [146]

Nowadays, most Cu-CHA zeolite catalysts are prepared by an ion-exchange method using Cu salt precursors and CHA zeolite supports, usually including ion-exchange, filtration, washing and calcination procedures. Due to the limits in channel size and exchange capacity of CHA zeolites, repeated ion-exchange procedures or longer ion-exchange time is necessary to increase the Cu loading. Furthermore, the synthesis of SSZ-13 zeolites requires the structure-directing agent (SDA) *N,N,N*-trimethyl-1-adamantammonium hydroxide (TMAdaOH), which is very expensive [152], limiting the wide application of this material in industry. Therefore, it is highly imperative to improve the synthesis method to reduce the cost of Cu-SSZ-13 catalysts for the NH_3-SCR process. Using the low-cost Cu-tetraethylenepentamine (Cu-TEPA) complex as a novel template, which is stable in strong alkaline solution and matches the CHA cage structure very well, Ren *et al.* [153, 154] successfully designed a one-pot synthesis method for Cu-SSZ-13 catalysts, obtaining products with high Cu loading and high dispersion of Cu species simultaneously. Through adjusting the starting compositions in the precursor gels, Cu-SSZ-13 zeolites with different Si/Al ratios could be synthesized. The preliminary results showed that the one-pot synthesized Cu-SSZ-13 catalyst exhibited very good NH_3-SCR activity, especially in the low temperature range, yet much more work should be done to investigate its feasibility in practical use for the deNO_x process of diesel engines. Picone *et al.* [155] used Cu cyclam (1,4,8,11-tetraazacyclotetradecane) and tetraethylammonium (TEA^+) acting as co-templates to directly synthesize a Cu-SAPO STA-7 catalyst with similar structure to that of Cu-SAPO-34, showing comparable performance in the NH_3-SCR reaction to that of Cu-ZSM-5 prepared by an ion-exchange method and higher performance than that of Cu-SAPO STA-7 with similar Cu content prepared by an aqueous ion-exchange method. The characterization results showed that a more homogeneous distribution of Cu species in Cu-SAPO STA-7 was achieved via direct synthesis, which was probably the main reason for its high deNO_x efficiency. The one-pot synthesis methods for Cu-based zeolite catalysts with small pore size using relatively cheap Cu-containing templates allow researchers to tune the Cu content, Cu distribution, and Si/Al ratio and thus the NH_3-SCR activity efficiently, although this approach is restricted to those zeolitic systems that can be prepared using coordination complexes as templates [156]. For practical use of this approach in industry, we believe, there is still a long but exciting way to go.

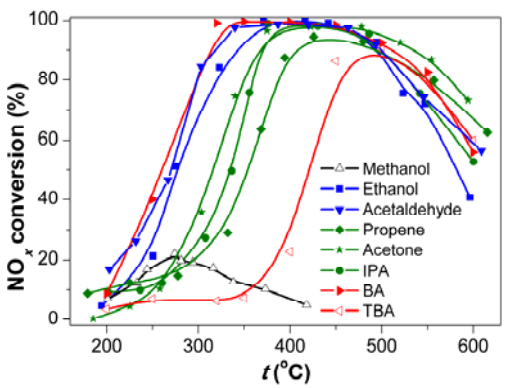

Fig. 2. Activity of 4 wt.% Ag/Al_2O_3 for NO_x conversion by various hydrocarbons at different temperatures. Conditions: NO 800 ppm, O_2 10%, H_2O 10%, reductants (methanol 3030 ppm, or ethanol 1565 ppm, or acetaldehyde 1565 ppm, or propene 1714 ppm, or acetone 1043 ppm, or

IPA 1043 ppm, or BA 783 ppm, or TBA 783 ppm), N_2 balance, total flow = 2000 ml min^{-1}, GHSV = 50,000 h^{-1}.

3. Mechanism responsible for the high performance of Ag/Al_2O_3 for the SCR of NO_x with oxygenated hydrocarbons

It has been widely accepted that the structure of hydrocarbons has a great influence on the activity of Ag/Al_2O_3 for NO_x reduction [13, 16, 157]. Oxygenated hydrocarbons such as ethanol, acetaldehyde, and propyl alcohol exhibit excellent NO_x reduction activity on Ag/Al_2O_3 [158, 159], which was also confirmed by our results [160-163]. More importantly, we attempted to determine the intrinsically property responsible for the NO_x reduction by oxygenated hydrocarbons over Ag/Al_2O_3. As shown in Fig. 2, methanol shows the poorest activity for NO_x reduction, while ethanol, acetaldehyde, and butyl alcohol (BA) are most active, giving similar T_{50} (50% NO_x conversion) at *ca.* 270 °C with a SV of 50000 h^{-1}. It be should noted that tert-butyl alcohol (TBA) exhibits a much lower NO_x conversion in the temperature range 200-450 °C, providing a T_{50} for NO_x conversion at around 420 °C, which is *ca.* 150 °C higher than that of the T_{50} with BA. The reductants with three carbon atoms (iso-propanol (IPA), and acetone) exhibit moderate activity for NO_x reduction. Clearly, both the carbon chain length and configuration of oxygenated hydrocarbons have a pronounced effect on their properties for NO_x reduction, therefore understanding such differences at the mechanism level may give clues for the design of a HC-SCR system with high efficiency.

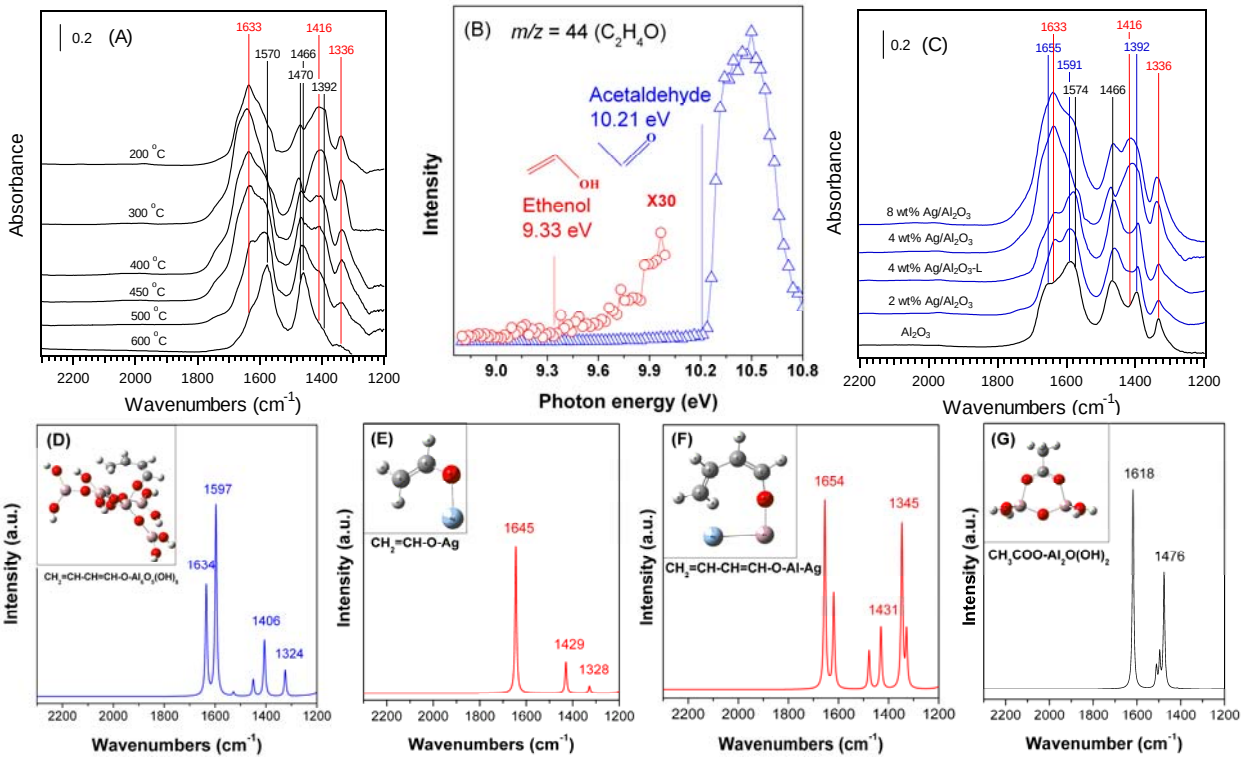

Fig. 3. (A) *in situ* DRIFTS spectra of 4 wt.% Ag/Al_2O_3 during partial oxidation of ethanol at different temperatures [162]; (B) The photoionization efficiency (PIE) spectra of m/z = 44 (C_2H_4O) measured in a flow of ethanol + O_2 over Ag/Al_2O_3 under low pressure at 330 °C [164]; (C) *in situ* DRIFTS spectra of Ag/Al_2O_3 with different Ag loadings during partial oxidation of ethanol at 250 °C; (D) molecular structure of the calculation model (inset figure) and its calculated FTIR spectrum for the surface C_4 enolic species on Al_2O_3; (E) surface C_2 enolic species on Ag/Al_2O_3; (F) C_4 enolic species on Ag/Al_2O_3 [165]; and (G) surface acetate on Ag/Al_2O_3 [166]. (Reproduced with permission from Elsevier Inc. and American Chemical Society)

3.1. Partial oxidation of oxygenated hydrocarbons over Ag/Al_2O_3

As the initial step of HC-SCR, the partial oxidation of hydrocarbons has attracted much attention. In NO_x reduction by ethanol over Ag/Al_2O_3, it has been proposed that acetate derived from the partial oxidation of ethanol plays a crucial role in the formation of isocyanate species (-NCO), as well as in the global NO_x reduction process [13, 30, 31, 167-169]. A possible mechanism for NO_x reduction by ethanol over Ag/Al_2O_3 was judged to be similar to that of C_3H_6: approximately, NO + O_2 + C_2H_5OH → NO_x (nitrate in particular) + $C_xH_yO_z$ (acetate in particular) → R-NO_2 + R-ONO → -NCO + -CN + NO + O_2 → N_2 [23, 24, 30, 31, 167-171]. However, this mechanism does not sufficiently explain why ethanol has a much higher efficiency for the SCR of NO_x over Ag/Al_2O_3 than hydrocarbons such as propene (Fig. 2).

In our earlier papers [162, 172, 173], the formation and dynamic performance of partial oxidation products of ethanol over Ag/Al_2O_3 were studied by an *in situ* DRIFTS method, and we found a novel enolic species originating from the partial oxidation of ethanol, with the structural feature of an oxygen atom adjacent to carbon-carbon double bonds (C=C-O). As shown in Fig. 3A, peaks at 1633, 1416 and 1336 cm^{-1} were assigned to the enolic species adsorbed on the surface of

Ag/Al_2O_3. This assignment was confirmed by using 2,3-dihydrofuran as an enolic model compound, which has a structure containing C=C bonded with an oxygen. From a comparison of the intensities of the respective peaks in Fig. 3A, we deduced that the enolic species is predominant during the oxidation of ethanol on the Ag/Al_2O_3 surface at low temperatures (within the range of 200-450 ^oC). However, at high temperatures ranging from 500 to 600 ^oC, the surface acetate species exhibiting characteristic frequencies at 1570 and 1466 cm^{-1} becomes dominant.

The partial oxidation intermediates of ethanol over Ag/Al_2O_3 were further identified by synchrotron vacuum ultraviolet (VUV) photoionization mass spectrometry (PIMS), and photoionization efficiency (PIE) spectra [164]. The PIE spectra of *m/z* = 44 (C_2H_4O) (Fig. 3B) at low pressure unambiguously illustrate the presence of ethenol (CH_2=CH-OH), with the ionization threshold of 9.33 eV [174]. At normal atmospheric pressure, however, this species was hardly observed in the gas phase, indicating a high level of activity. This result also indicates that Ag/Al_2O_3 provides a suitable surface to stabilize the ethenol, because of its strong DRIFTS intensity on the catalyst surface under normal pressure (Fig. 3A). Acetaldehyde, as the stable isomer of ethenol, was detected under low and atmospheric pressure with high ion intensity, giving the characteristic threshold of 10.21 eV.

Meanwhile, propenal (CH_2=CHCHO), acetone (CH_3COCH_3), and 2-butenal (CH_3CH=CH-CHO) were also measured by VUV-PIMS during the partial oxidation of ethanol over Ag/Al_2O_3. This indicates that a condensation reaction occurs synchronously during the partial oxidation of ethanol over Ag/Al_2O_3, which also agrees with our TPD-MS experiment [173]. The condensation reactions of aldehydes, as well as ketones, are widely used in organic synthesis and are commonly catalyzed by zeolites, Al_2O_3, and TiO_2 [175-177].

On a detailed mechanistic level, the role of silver species in the HC-SCR of NO_x over Ag/Al_2O_3 was mainly attributed to enhancement of the partial oxidation of reductants to form active intermediates, and their further reaction to produce N_2 [16, 158, 172, 178]. *In situ* DRIFTS spectra showed that the surface species formed from the partial oxidation of ethanol over Ag/Al_2O_3 (Fig. 3C) were closely related to Ag loading [165]. Over pure Al_2O_3, the surface enolic species adsorbed on Al sites exhibited characteristic peaks at 1655, 1591, 1392, and 1336 cm^{-1}. After Ag loading, the peaks due to enolic species were observed at 1633, 1416, and 1336 cm^{-1}, the intensity of which gradually increased with increasing Ag content, indicating that this species would be bound on or close to Ag sites.

Density functional theory (DFT) calculations were also used to confirm the structure of adsorbed enolic species and acetate on Ag/Al_2O_3 [162, 165, 166, 173, 179]. Two kinds of surface enolic species, adsorbed only on Al sites (CH_2=CH-CH=CH-O-$Al_6O_5(OH)_8$) and bound on or close to Ag (CH_2=CH-O-Ag, CH_2=CH-CH=CH-O-Al-Ag) were suggested by DFT calculations over Ag/Al_2O_3 and Al_2O_3, with the simulation molecular structure model and corresponding FTIR spectrum shown in Fig. 3D, 3E, and 3F, respectively [165]. As revealed by ICP measurements [165], the molar ratio of Al/Ag on 4 wt.% Ag/Al_2O_3 was as high as 60, while enolic species bound on Al sites were hardly observed (Fig. 3C), strongly suggesting that the enolic species is preferably adsorbed on or close to silver sites.

On all Ag/Al_2O_3 samples, UV-vis analysis shows that that Ag species are mainly present in the oxidized state (Ag^+ and $Ag_n^{\delta+}$) [40, 180-184]. Kinetic measurements confirm that such silver species, particularly strongly bound Ag^+ ions, are the active sites responsible for the reduction of NO_x with ethanol. Thus, we propose that the enolic species on the Ag/Al_2O_3 surface possibly adsorb on or close to isolated Ag^+ ions and/or $Ag_n^{\delta+}$ clusters, exhibiting an intimate contact with the active phase. This enolic species was clearly observed on the leached sample (Fig. 3C), in which Ag^+ ions were predominant, further supporting our assumption [165]. By using precipitable silver compound supported catalysts such as Ag_3PO_4/Al_2O_3, Ag_2SO_4/Al_2O_3 and $AgCl/Al_2O_3$, we also confirmed that the high dispersion Ag^+ cations were the active silver species for NO_x reduction by ethanol, on which the reactive enolic species was formed having strong infrared intensity in the typical temperature range of 250-500 ^oC [185].

During the partial oxidation of ethanol on all samples, meanwhile, the peaks due to surface acetate were also clearly observed, with the characteristic vibrational frequencies (1574 and 1466 cm^{-1}), regardless of silver loading. These results indicate that the acetate species formed during the partial oxidation of ethanol may mainly adsorb on Al sites instead of Ag sites. The adsorption characteristics of acetate on the surface of Ag/Al_2O_3 catalysts have also been investigated by DFT calculations [166]. The calculated vibrational spectrum of acetate adsorbed on Al sites, present as CH_3COO-$Al_2O(OH)_2$, is in good agreement with the experimental one (Fig. 3G), while there is a large error between the calculated and experimental vibrational modes of the acetate species bound on silver sites, further confirming that acetate species over Ag/Al_2O_3 are prone to interact with Al sites.

Based on the above results, the formation mechanism for surface enolic species during the partial oxidation of ethanol over Ag/Al_2O_3 was proposed as shown in Scheme 5. Ethanol principally reacts with oxygen to form acetaldehyde, which is followed by isomerization to ethenol. Subsequently, a C_2 enolic anion (CH_2=CH-O^-)-M^+ is formed by hydrogen extraction when ethenol is adsorbed on the surface of Ag/Al_2O_3. Meanwhile, the occurrence of aldol condensation of acetaldehyde, which has been confirmed by PIMS and TPD-MS measurement, may lead to the formation of C_4 enolic species (CH_2=CH-CH=CH-O^-)-M^+ as shown in Scheme 5 [164, 173].

Obviously, if the formation of surface enolic species follows the hypothesis described above, two prerequisites must be met. First, the selected reductant must contain at least one C-C bond. This has been clarified by our previous research, in which the enolic species was rarely observed when CH_3OH (Fig. 4A) and CH_3OCH_3 were partially oxidized over Ag/Al_2O_3 [161, 186]. Secondly, it is widely accepted that the structural feature H-C-O-H is required for the partial oxidation of alcohols to aldehydes and/or ketones. That is, the OH group must be attached to a carbon atom with at least one hydrogen atom (denoted as α-H). Considering that enols are the tautomers of aledhyde/ketones, the presence of α-H is also a prerequisite for the formation of enolic species during partial oxidation of alcohols over Ag/Al_2O_3. To highlight this issue, butyl alcohol isomers with and without α-H were employed as reductants for NO_x reduction over 4 wt.%

Ag/Al_2O_3 [163]. 1-butanol (Fig. 4B), sec-butyl alcohol and isobutyl alcohol, containing α-H, are favorable for the partial oxidation to form enolic species while the α-H participated reaction pathway is impossible for tert-butyl alcohol (Fig. 4C) due to the absence of α-H.

Previous research further identified that surface enolic species were also produced during the partial oxidation of 1-propanol (and isopropyl alcohol) over Ag/Al_2O_3 [160, 161, 187], acetaldehyde over both Ag/Al_2O_3 [172] and Co/Al_2O_3 [188], and acetylene over ZSM-5 [189]. Interestingly, substantial quantities of enols in the gas phase have been observed by VUV-PIMS during the combustion of hydrocarbons [190]. The above results strongly suggest that adsorbed enolic species and/or enols in the gas phase are common intermediates involved in the partial oxidation of hydrocarbons and oxygenated hydrocarbons. As a result, identification of their role is a key point in understanding of the pathway of HC-SCR.

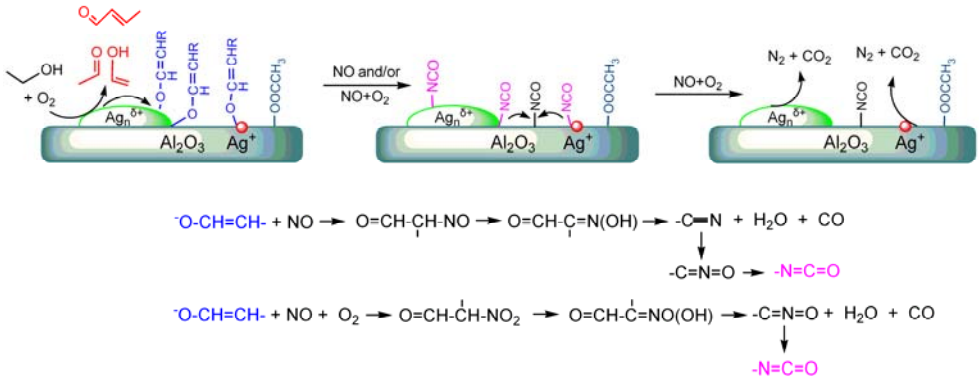

Scheme 5. Hypothesis for adsorbed enolic species formation and mechanism of ethanol-SCR of NO_x over Ag/Al_2O_3. The intermediates in the gas phase such as acetaldehyde, ethenol, and 2-butenal were confirmed by VUV-PIMS measurement [164]. Surface enolic species, acetate, and -NCO were identified by DRIFTS and DFT calculations [165, 173]. (Reproduced with permission from Elsevier Inc.) [165]

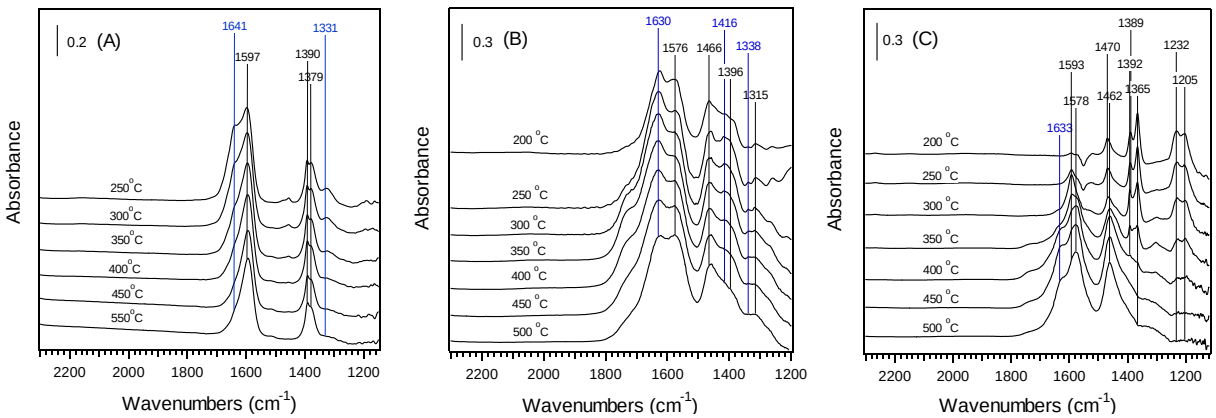

Fig. 4. *In situ* DRIFTS spectra of 4 wt.% Ag/Al_2O_3 during partial oxidation of methanol (A) [161], 1-butanol (B) [163], and tert-butyl alcohol (C) [163] at different temperatures. Conditions: the concentrations of reductants are the same as Fig. 2, O_2 10%, N_2 balance. (Reproduced with permission from Elsevier Inc.)

3.2. Reactivity of intermediates originating from partial oxidation of oxygenated hydrocarbons over Ag/Al_2O_3

It has been widely accepted that the -NCO species is a vital intermediate for the SCR of NO_x with ethanol and other hydrocarbons, thus much attention has focused on its formation and reactivity [29, 178, 191-197]. With this in mind, the relationship between -NCO formation and the consumption of enolic species and acetate was investigated on Ag/Al_2O_3 via the transient response of the DRIFTS method, and typical results are presented in Fig. 5 [165].

After exposure of 4 wt.% Ag/Al_2O_3 to $C_2H_5OH + O_2$ at 400°C for 60 min, the enolic species bound on or close to Ag sites exhibited strong peaks at 1633, 1412, and 1338 cm^{-1}, while the characteristic vibration modes of the enolic species adsorbed on Al sites were hardly observed. Strong peaks assignable to acetate were also observed at 1573 and 1466 cm^{-1} (Fig. 5A). Switching the feed gas to NO resulted in a significant decrease in the intensity of peaks due to enolic species, while the decrease in the intensity of acetate peaks was much slower than that of enolic species on the same time scale. Meanwhile, this decrease was accompanied by the appearance of peaks due to -NCO, whose intensity increased with time on stream. These results confirm that the enolic species bound on or close to Ag sites are more active toward NO to form -NCO than is acetate at this temperature (Fig. 5B).

Under the same conditions as in the above experiments, we also analyzed the reactivity of enolic species and acetate when NO + O_2 was introduced over 4 wt.% Ag/Al_2O_3 (Fig. 5C and 5D). In this case, a more significant decrease in the concentration of enolic species was observed compared with experiments carried out in the absence of O_2. The trend of -NCO with time on stream follows the typical behavior of a reactive intermediate, increasing its intensity at the beginning, reaching a maximum at 3 min and then decreasing gradually. Meanwhile, the gas phase products such as N_2 and CO_2 were measured by mass spectrometry, with results shown in Fig. 5E. Based on these data, the consumption of surface enolic species within 25 min was estimated at 283.1-566.2 μmol/g-cat, which is fairly close to that of the final product N_2, 204.5 μmol/g-cat. These results quantitatively confirm that the enolic species in intimate contact with the active phase plays a crucial role in the reduction of NO_x with ethanol. Over this catalyst, meanwhile, H_2-O_2 titration showed that the accessible amount of silver sites was 85.34 μmol/g-cat, which is lower than that of surface enolic species. This result indicates that not only the Ag sites, but also Al sites closely linked to Ag participate in the formation of surface enolic species, further confirming our assignment for this species.

Further studies confirmed that the enolic species originating from the partial oxidation of butyl alcohol (BA), sec-butyl alcohol (SBA), and isobutyl alcohol (IBA), propyl alcohol [160], isopropyl alcohol (IPA) [161], and acetaldehyde [162] over Ag/Al_2O_3 also exhibited high activity toward NO + O_2, and thus are responsible for NO_x reduction by these oxygenated hydrocarbons.

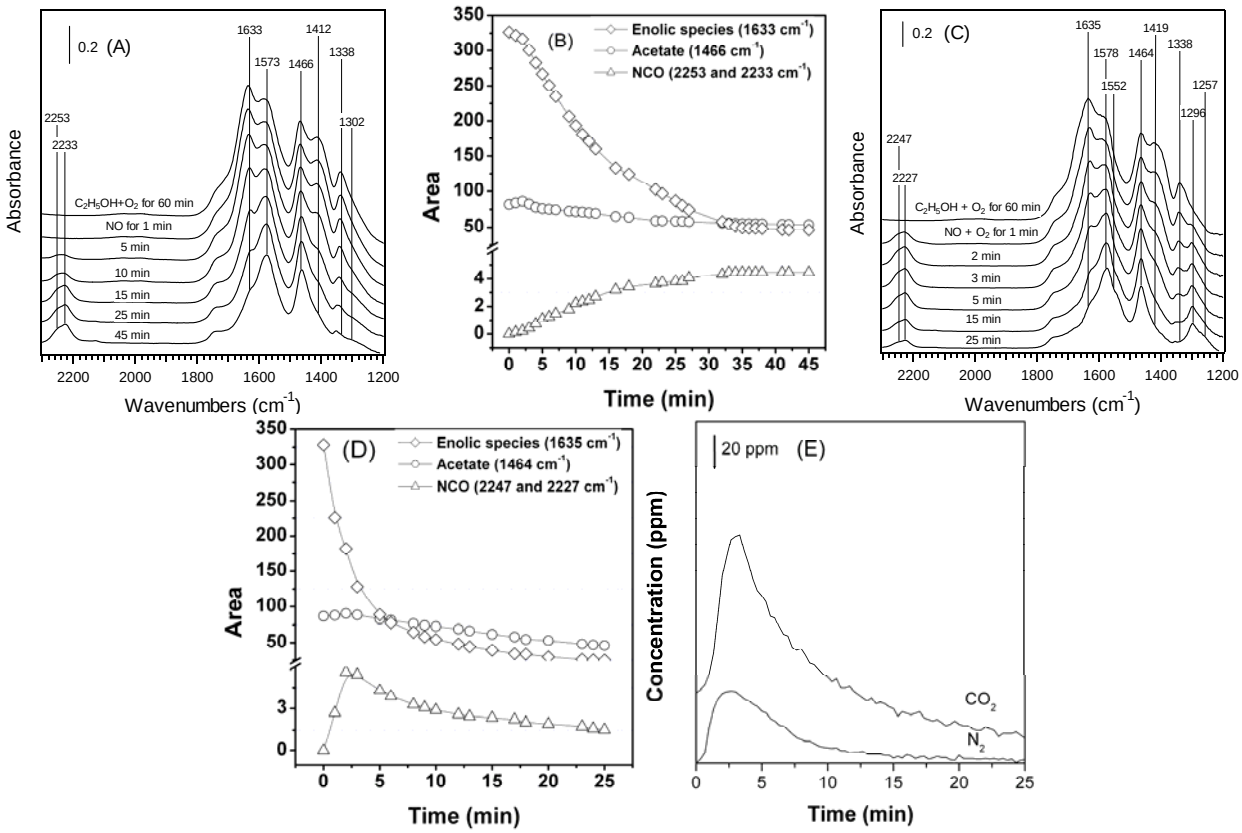

Fig. 5. Dynamic changes of *in situ* DRIFTS spectra over 4 wt.% Ag/Al_2O_3 as a function of time in a flow of NO (A), and in a flow of NO + O_2 at 400 °C. Before measurement, the catalyst was pre-exposed to a flow of C_2H_5OH + O_2 for 60 min at 400 °C. Conditions: NO 800 ppm, C_2H_5OH 1565 ppm, O_2 10% (if used), N_2 or Ar (for the case of (B)) balance. (C) and (D) time dependence of the integrated areas of the peaks of enolic species (◊), acetate (○), and -NCO (Δ) for the cases of (A), and (B), respectively, and (E) time dependence of N_2 and CO_2 concentration calculated from the mass signals for the cases of (C). (Reproduced with permission from Elsevier Inc.) [165]

3.3. Reaction pathway of HC-SCR over Ag/Al_2O_3

Based on the above results, a mechanism for the NO_x reduction by ethanol over Ag/Al_2O_3 was proposed as shown in Scheme 5. In a typical reaction process, partial oxidation of ethanol results in the formation of enolic species adsorbed on Al and Ag sites, as well as the formation of acetate on Al sites. Such different features in the adsorption sites for the enolic and acetate species on Ag/Al_2O_3 may contribute to their different reactivity toward NO + O_2 (and/or NO), and their role in the formation of -NCO during the reduction of NO_x with ethanol. The enolic species intimately linked with Ag sites (RCH=CH-O-Ag and RCH=CH-O-Al-Ag), possessing high activity, further react with NO + O_2 (and/or NO), to form Ag-NCO. The acetate bound on Al sites are less active when compared with the enolic species intimately linked with Ag sites, and thus play a minor role in -NCO formation. With an increase in the concentration of Ag-NCO, this

species can transfer to Al sites, and as a result, the characteristic frequency of Al-NCO can be observed by the DRIFTS method.

The characteristic IR peaks of -NCO located around 2230 and 2250-2260 cm^{-1} have been commonly observed on Ag/Al_2O_3 during HC-SCR, while the assignments of their coordination sites are still controversial. Bion *et al.* [191, 192], and Thibault-Starzyk *et al.* [196] observed the characteristic frequencies of -NCO on Ag/Al_2O_3 located at 2255-2265 and 2228-2240 cm^{-1}, which were assigned to -NCO species coordinated with octahedral Al^{3+} ions (Al^{VI}-NCO) and tetrahedral Al^{3+} sites (Al^{IV}-NCO), respectively. During the reduction of NO_x with ethanol and propene on Ag/Al_2O_3, the two peaks at 2258-2262 and 2230-2235 cm^{-1} were detected by Ukisu *et al.* [198], Kameoka *et al.* [23, 199], and Sumiya *et al.* [29, 168]. The high-frequency peak was assigned to Al-NCO, while the low-frequency one was attributed to adsorption on Ag sites (Ag-NCO). To identify the adsorption sites of -NCO on the Ag/Al_2O_3 surface, DFT calculations were performed by Gao and He [194]. The calculated results indicate that the antisymmetric stretching mode of the Al-NCO group is located at 2267 cm^{-1} with strong intensity, which is in excellent agreement with the experimental value (around 2260 cm^{-1}). The calculated mode of $(OH)_2$Al-O-Ag-NCO shows the asymmetric stretching frequency of -NCO at 2215 cm^{-1}, also close to the corresponding experimental one (around 2230 cm^{-1}), indicating that the low-frequency peak may correspond to the -NCO species adsorbed on or close to Ag sites. Because of the weak intensity, the symmetric stretching mode for the surface structure containing Ag-NCO or Al-NCO groups has not been observed in the experimental IR spectra, which has also been proved by the DFT calculation. By using an elegant short time-on-stream *in situ* spectroscopic transient isotope experimental technique, more recently, Chansai *et al.* [178, 200] proposed that there may be two types of -NCO species during the reduction of NO_x with hydrocarbons over Ag/Al_2O_3. One is a slowly reacting spectator -NCO species, probably adsorbed on the oxide support of Al_2O_3, while another is related to reactive -NCO, possibly on or close to the active silver phase.

Organo-nitrite and -nitro species (R-ONO and R-NO_2) have been regarded as potential intermediates in the SCR of NO_x with hydrocarbons, which contributed to the formation of -NCO by reaction between the partial oxidation products of hydrocarbons and NO_x (or ad-NO_x) [201]. As for ethanol-SCR over Ag/Al_2O_3, the two species may also participate the formation of -NCO during exposure of the surface enolic species to NO and/ NO + O_2. In organic synthesis, enols and/or enolate anions are common intermediates in nitrosation reactions between aldehydes/ketones and substrates containing the NO group such as HONO, NO^+, NO^-, neutral NO, $C(NO_2)_4$, and $[Fe(CN)_5NO]_2^-$ to form the initial product of nitroso and nitro compounds [202-204]. This mechanism permitted us to hypothesize that similar reactions would occur during exposure of enolic species to NO on Ag/Al_2O_3, resulting in the formation of an organo-nitrite compound. Transformation of this organo-NO_x compound to its enol tautomer, -CH=N(OH), with subsequent dehydration to -CN and transformation to -NCO, has been proposed as a possible route for -NCO formation [181, 191, 205]. The presence of O_2 promoted the reaction of enolic species toward NO, possibly resulting in the formation of an organo-nitro intermediate. This compound was also contributed to produce -NCO *via* enol and -CNO formation [181, 191, 205].

A general reaction pathway involving the formation of enolic species closely linked to active Ag sites was proposed to explain the NO_x reduction by different alcohols over Ag/Al_2O_3 [206]. As shown in Scheme 6, both the presence of α-H and at least C=C bond in alcohols are necessary for the formation of enolic species. The employed alcohols with these two features thus exhibit high efficiency for NO_x reduction, derived from the high concentration of reactive enolic species. As for NO_x reduction by hydrocarbons such as alkanes and alkenes, however, the formation of acetate (or formate in the case of NO_x reduction by CH_4) and its further transformation to -NCO play a crucial role in NO_x reduction. The low reactivity of acetate (or formate) results in a low efficiency for NO_x reduction by hydrocarbons if compared with the NO_x reduction by oxygenated hydrocarbons such as ethanol.

Water vapor is commonly present in diesel engine exhaust, the presence of which has a great influence on the reaction pathway of the HC-SCR [13, 158, 191]. Generally, the presence of water vapor usually suppressed the NO_x reduction by hydrocarbons such as propene over Ag/Al_2O_3, while high NO_x conversion was maintained when oxygenated hydrocarbons such as ethanol were employed as reductants. In our previous work [16], *in situ* DRIFTS results showed that the presence of water vapor promoted the formation of enolic species intimately linked to Ag sites, while it suppressed the formation of acetate species. These opposite effects of water vapor on the two species may derive from their different behaviors on the adsorbed sites, identification of which may provide important implications for understanding the effect of water vapor on the HC-SCR.

From a practical point of view, it is important to develop catalysts or catalyst-reductant systems that are active for NO_x reduction in the presence of SO_2. Numerous studies confirmed that the structure of hydrocarbons (oxygenated hydrocarbons) was not only responsible for the activity of Ag/Al_2O_3 for NO_x reduction, but also contributed to the sulfur tolerance of this silver catalyst [13, 159, 160]. In the presence SO_2, the deteriorated activity of Ag/Al_2O_3 for HC-SCR was mainly due to the adsorption and accumulation of sulfates on the Al_2O_3 support, before which the oxidation of SO_2 should have occurred on Ag sites [13, 207, 208]. As for NO_x reduction by oxygenated hydrocarbons such as ethanol and acetaldehyde, large amounts of enolic species were formed, which adsorbed on or close to the active Ag sites. On the Ag sites covered with enolic species, the oxidation of SO_2 would be suppressed, followed by the adsorption and accumulation of sulfates. Therefore, it is reasonable that the catalyst-reductant system of Ag/Al_2O_3-oxygenated hydrocarbon exhibits high sulfur tolerance. The acetate, as the main product of partial oxidation of hydrocarbons, prefers to interact with Al sites. This situation is of benefit for SO_2 oxidation on Ag sites, and thus a pronounced poisoning effect would be observed during NO_x reduction by hydrocarbons such as C_3H_6 over Ag/Al_2O_3.

Recently, it was found that the presence of H_2 significantly enhanced the low temperature activity of Ag-based catalysts for NO_x reduction by hydrocarbons [17, 40, 209-211]. Up to now, however, the interpretation of the H_2 promotional effect on HC-SCR has been under debate. To increase the rate of NO_x conversion,

basically, the hydrogen must accelerate the rate(s) of the slow step(s) in the reaction of HC-SCR, while the slow step(s) are likely to vary depending on the reaction temperature and feed conditions [212]. We were the first to report the pronounced promotional effect of H_2 on the NO_x reduction by ethanol over Ag/Al_2O_3 even in the presence of water vapor [213]. Evidence provided by *in situ* DRIFTS revealed that the presence of H_2 enhanced the formation of enolic species during the partial oxidation of ethanol over Ag/Al_2O_3 at low temperatures. Such enhancement by H_2 was also confirmed by GC-MS analysis, by promoting the formation of organic nitrogen-containing intermediates such as CH_3-NO_2 and CH_3CN during the ethanol-SCR over Ag/Al_2O_3 at low temperatures. By using *in situ* DRIFTS, we also found that the presence of H_2 increased the activity of -NCO toward NO + O_2 during the NO_x reduction by ethanol over Ag/Al_2O_3. As revealed by VUV-PIMS analysis, meanwhile, the presence of H_2 may trigger the hydrolysis of -NCO to NH_3, providing a new pathway for NO_x reduction [206]. As a result, we proposed that the H_2 effect on ethanol-SCR could be attributed to enhancement of the formation of enolic species and their further transformation to -NCO *via* the formation of organic nitrogen-containing species, which has been presented in Scheme 6. Such enhancement was also observed during the NO_x reduction by C_3H_6 over Ag/Al_2O_3 in the presence of H_2 [160, 214].

Scheme 6. Mechanism of HC-SCR of NO_x over Ag/Al_2O_3 (Reproduced with permission from CAS/DICP) [206]

Typically, most of the studies dealing with the reaction mechanism of HC-SCR have been restricted to surface phenomena. However, Eränen and co-workers [215, 216] proposed that the octane-SCR over Ag/Al_2O_3 not only occurs on the surface of catalyst but also continues in the gas phase, leading to the final products of N_2, H_2O, CO_2. Such gas-phase reaction was proved by placing a commercial Pt-supported oxidation catalyst after the Ag/Al_2O_3 catalyst in order to remove CO and unburnt hydrocarbons. When the oxidation catalyst was placed immediately behind the Ag/Al_2O_3, NO_x conversion to N_2 was decreased dramatically. Similar gas-phase reaction was also observed to occur during NO_x reduction by ethanol over Ag/Al_2O_3 [24, 217, 218]. The above results strongly suggest that very active N-containing intermediates in the gas phase were created over the Ag/Al_2O_3 catalyst. Identification of these unstable intermediates is thus important in order to understand the mechanism of HC-SCR over Ag/Al_2O_3 and to further optimize the catalysts. However, this may be a difficult task because these gas phase intermediates possess very high reactivity and a short lifetime. Eränen *et al.* [215] proposed that gas phase reaction behind the silver catalyst may be involved in the reaction of activated NO_x species with amines and ammonia. Organic N-containing species such as R-NO_2, R-NCO, and R-CN are intermediates in the formation of amines and ammonia, which may also take part in this gas reaction. Using a conventional electron-impact (EI) ionization mass spectrometer and liquid nitrogen trap, unfortunately, only R-CN species were detected during the NO_x reduction by octane over Ag/Al_2O_3, together with nitrogen-free species due to the partial oxidation of the reductant [215]. During the NO_x reduction by ethanol or octane over Ag/Al_2O_3, large amounts of N-containing species such as NH_3 and HCN were detected by a conventional MS technique [24]. Considering that the two gas phase species are not so active as to produce N_2 in a catalyst-free system, this may not be the true story. Indeed, the real intermediates would have changed into the final product of N_2 and/or more stable species owing to molecular collision and secondary reaction during the sampling and long retention times of a conventional mass spectrometer.

Recently, synchrotron vacuum ultraviolet (VUV) photoionization combined with molecular-beam mass spectrometry (MBMS), also referred to as synchrotron VUV photoionization mass spectrometry (VUV-PIMS), was successfully applied in detecting reactive intermediates in hydrocarbon combustion chemistry [190, 219]. In this case, molecular-beam sampling and high vacuum downstream can ensure free molecular flow of the sampled gas and reduce collision effects, making it possible to detect both stable and unstable intermediates; the employed vacuum ultraviolet single-photon photoionization can minimize fragmentation of target molecules because the total absorbed photon energy barely exceeds the ionization energy. Both of these two advantages of VUV-PIMS may also provide an opportunity for identification of the reactive gas phase intermediates created by Ag/Al_2O_3 during the HC-SCR and give deeper insight into its mechanism if this technique is employed properly. In fact, by using this powerful method, ethenol in gas phase, an important intermediate during the catalytic oxidation of C_2-C_4 alcohols over Ag/Al_2O_3 catalyst, was unambiguously identified [164, 219], further confirming the formation of surface enolic species during the NO_x reduction by ethanol over Ag/Al_2O_3.

4. Conclusions and perspectives

The development of vanadium-free catalysts for the NH_3-SCR of NO_x with high deNO_x activity, N_2 selectivity, hydrothermal

stability and durability toward poisoning components is a continuing research hotspot in the field of environmental catalysis. The study of the structure-activity relationship of these environmentally-benign catalysts in the NH_3-SCR reaction shows that the high dispersion of active species is a very important factor influencing the SCR performance, not only for metal oxide catalysts (such as the high dispersion of Fe^{3+}-$(O)_2$-Ti^{4+} species in the $FeTiO_x$ catalyst and CeO_x species in $CeTiO_x$, $CeWTiO_x$ and $CeWO_x$ catalysts), but also for zeolitic catalysts (such as the isolated Fe^{3+} and Cu^{2+} species located in ion-exchanged sites), which is a quite common view in heterogeneous catalysis. For metal oxide catalysts, the investigation of the effect of exposing different crystal facets in the NH_3-SCR reaction, especially for Fe_2O_3 oxides, has achieved great success, which may be extended to other metal catalyst systems for better understanding of the intrinsic origin of excellent SCR performance on certain materials. The improvement of hydrothermal stability is highly needed for metal oxide NH_3-SCR catalysts, and is a main factor restricting their practical use in the deNO_x process of diesel engines. Although the hydrothermal stability of Fe- and Cu-based zeolite catalysts is higher to a certain extent, due to the long-term operating conditions involving water vapor and timed thermal shock, the migration of isolated active sites still can occur, which requires researchers to develop novel zeolitic materials to meet the increasingly strict NO_x emission standards. The Cu-CHA catalysts such as Cu-SSZ-13, Cu-SAPO-34 and Cu-AEI catalyst such as Cu-SSZ-39 are good examples in this field, and we believe in the near future, more and more novel, efficient zeolitic materials will be developed not only by conventional ion-exchange, chemical vapor deposition methods *etc.* but also by one-pot synthesis using cheaper templates.

The acidity of NH_3-SCR catalysts is always given close attention by researchers, although many debates still remain. On metal oxide catalysts, both the Brønsted acid sites and Lewis acid sites are usually considered to be involved in the NH_3-SCR process, while on zeolite catalysts, only the Brønsted acid sites are proven to be useful for holding active metal sites and storing the reducing agent NH_3. The differences in understanding of the effects of acid sites on metal oxide catalysts and zeolite catalysts may be due to the distinct dispersion, microstructure and neighboring local environments of active sites in these two types of materials. For the metal oxide catalysts, with their relatively large amount of active phase but small amount of acid sites, the proper increase in acidity may be helpful for the deNO_x process; while for the zeolite catalysts, with relatively small quantities of isolated active sites but large amount of acid sites, maintaining the active sites in an isolated state is quite important. In further study, with more advanced methods including *ex situ, in situ,* and *operando* methods, we believe that a universally accepted structure-activity relationship for these vanadium-free catalysts for NH_3-SCR reaction can be established.

The HC-SCR of NO_x has attracted much attention as a possible alternative to the NH_3/Urea-SCR. However, the activity and/or stability of catalysts developed for diesel-SCR are not sufficient to satisfy the demanding conditions of the deNO_x application for diesel engines. On the other hand, the oxygenated hydrocarbons such as ethanol, acetaldehyde, propyl alcohols, and butyl alcohols exhibit excellent NO_x reduction activity on Ag/Al_2O_3, during which enolic species were formed and identified by *in situ* DRIFTS, VUV-PIMS measurements and DFT calculation. The enolic species originating from the partial oxidation of alcohols over Ag/Al_2O_3 prefer to adsorb on or close to silver sites, in intimate contact with the active phase. This adsorption behavior of the enolic species contributes to their high activity for the formation of -NCO species and the final product N_2 during the NO_x reduction by oxygenated hydrocarbons over Ag/Al_2O_3. A general reaction pathway involving the formation of enolic species closely linked to active Ag sites was proposed to explain the NO_x reduction by different alcohols over Ag/Al_2O_3. The presence of at least one α-H and one C-C bond is indispensable for the employed alcohols to produce enolic species during their partial oxidation over Ag/Al_2O_3. This intrinsic property responsible for NO_x reduction by oxygenated hydrocarbons may provide a guideline for developing diesel-SCR of NO_x systems with high efficiency for diesel engines.

5. Acknowledgements

The authors give their sincere thanks for the support from the National Natural Science Foundation of China (51221892, 51108446, 21177142, 51278486) and the Ministry of Science and Technology, China (2013AA065301, 2010CB732304).

Notes and references

Research Center for Eco-Environmental Sciences, Chinese Academy of Sciences, Beijing 100085, P.R. China.
† *Authors made equal contributions.*
* *Corresponding author. Fax: 86-10-6284-9123; Tel: 86-10-6284-9123; E-mail: honghe@rcees.ac.cn*

1. H. Bosch and Janssen, F., *Catal. Today*, 1988, **2**, 369.
2. K. Skalska, J. S. Miller and S. Ledakowicz, *Sci. Total Environ.*, 2010, **408**, 3976.
3. P. Granger and V. I. Parvulescu, *Chem. Rev.*, 2011, **111**, 3155.
4. Z. Liu and S. Ihl Woo, *Catal. Rev.*, 2006, **48**, 43.
5. V. I. Pârvulescu, P. Grange and B. Delmon, *Catal. Today*, 1998, **46**, 233.
6. G. Busca, L. Lietti, G. Ramis and F. Berti, *Appl. Catal. B: Environ.*, 1998, **18**, 1.
7. S. Roy, M. S. Hegde and G. Madras, *Appl. Energy*, 2009, **86**, 2283.
8. T. V. Johnson, *Int. J. Engine Res.*, 2009, **10**, 275.
9. F. Liu, W. Shan, X. Shi, C. Zhang and H. He, *Chin. J. Catal.*, 2011, **32**, 1113.
10. S. Brandenberger, O. Kröcher, A. Tissler and R. Althoff, *Catal. Rev.*, 2008, **50**, 492.
11. M. Iwamoto, H. Yahiro, Y. Yu-u, S. Shundo and N. Mizuno, *Shokubai (Catalyst)*, 1990, **1990**, 430.
12. W. Held, A. König, T. Richter and L. Pupper, *SAE Paper*, 1990, 900496.
13. R. Burch, J. P. Breen and F. C. Meunier, *Appl. Catal. B: Environ.*, 2002, **39**, 283.
14. A. Fritz and V. Pitchon, *Appl. Catal. B: Environ.*, 1997, **13**, 1.
15. M. A. Gómez-García, V. Pitchon and A. Kiennemann, *Environ. Int.*, 2005, **31**, 445.
16. H. He and Y. Yu, *Catal. Today*, 2005, **100**, 37.
17. F. Klingstedt, K. Arve, K. Eränen and D. Y. Murzin, *Accounts Chem. Res.*, 2006, **39**, 273.
18. P. G. Savva and C. N. Costa, *Catal. Rev.*, 2011, **53**, 91.
19. K.-i. Shimizu and A. Satsuma, *Phys. Chem. Chem. Phys.*, 2006, **8**, 2677.
20. R. Burch and P. J. Millington, *Catal. Today*, 1995, **26**, 185.
21. J. Li, J. Hao, L. Fu, T. Zhu, Z. Liu and X. Cui, *Appl. Catal. A: Gen.*, 2004, **265**, 43.
22. K. A. Bethke and H. H. Kung, *J. Catal.*, 1997, **172**, 93.

23. S. Kameoka, Y. Ukisu and T. Miyadera, *Phys. Chem. Chem. Phys.*, 2000, **2**, 367.
24. J. H. Lee, S. J. Schmieg and S. H. Oh, *Appl. Catal. A: Gen.*, 2008, **342**, 78.
25. L. E. Lindfors, K. Eränen, F. Klingstedt and D. Y. Murzin, *Top. Catal.*, 2004, **28**, 185.
26. A. Martínez-Arias, M. Fernández-García, A. Iglesias-Juez, J. A. Anderson, J. C. Conesa and J. Soria, *Appl. Catal. B: Environ.*, 2000, **28**, 29.
27. V. I. Pârvulescu, B. Cojocaru, V. Pârvulescu, R. Richards, Z. Li, C. Cadigan, P. Granger, P. Miquel and C. Hardacre, *J. Catal.*, 2010, **272**, 92.
28. K.-i. Shimizu, A. Satsuma and T. Hattori, *Appl. Catal. B: Environ.*, 2000, **25**, 239.
29. S. Sumiya, H. He, A. Abe, N. Takezawa and K. Yoshida, *J. Chem. Soc., Faraday Trans.*, 1998, **94**, 2217.
30. Y. F. Tham, J. Y. Chen and R. W. Dibble, *P. Combust. Inst.*, 2009, **32**, 2827.
31. Y. H. Yeom, M. Li, W. M. H. Sachtler and E. Weitz, *J. Catal.*, 2006, **238**, 100.
32. D. Y. Yoon, J.-H. Park, H.-C. Kang, P. S. Kim, I.-S. Nam, G. K. Yeo, J. K. Kil and M.-S. Cha, *Appl. Catal. B: Environ.*, 2011, **101**, 275.
33. K. Arve, H. Backman, F. Klingstedt, K. Eränen and D. Y. Murzin, *Appl. Catal. B: Environ.*, 2007, **70**, 65.
34. V. Houel, P. Millington, R. Rajaram and A. Tsolakis, *Appl. Catal. B: Environ.*, 2007, **73**, 203.
35. M. K. Kim, P. S. Kim, J. H. Baik, I.-S. Nam, B. K. Cho and S. H. Oh, *Appl. Catal. B: Environ.*, 2011, **105**, 1.
36. T. Nakatsuji, R. Yasukawa, K. Tabata, K. Ueda and M. Niwa, *Appl. Catal. B: Environ.*, 1998, **17**, 333.
37. C. Petitto, H. P. Mutin and G. Delahay, *Chem. Commun.*, 2011, **47**, 10728.
38. J. Rodríguez-Fernández, A. Tsolakis, M. Ahmadinejad and S. Sitshebo, *Energ. Fuels*, 2009, **24**, 992.
39. B. Sawatmongkhon, A. Tsolakis, S. Sitshebo, J. Rodríguez-Fernández, M. Ahmadinejad, J. Collier and R. R. Rajaram, *Appl. Catal. B: Environ.*, 2010, **97**, 373.
40. P. Sazama, L. Čapek, H. Drobná, Z. Sobalík, J. Dědeček, K. Arve and B. Wichterlová, *J. Catal.*, 2005, **232**, 302.
41. C. L. DiMaggio, G. B. Fisher, K. M. Rahmoeller and M. Sellnau, *SAE paper*, 2009, 2009-01-0277.
42. A. Kato, S. Matsuda, F. Nakajima, M. Imanari and Y. Watanabe, *J. Phys. Chem.*, 1981, **85**, 1710.
43. J. P. Chen, M. C. Hausladen and R. T. Yang, *J. Catal.*, 1995, **151**, 135.
44. P. Fabrizioli, T. Bürgi and A. Baiker, *J. Catal.*, 2002, **206**, 143.
45. H. Teng, L.-Y. Hsu and Y.-C. Lai, *Environ. Sci. Technol.*, 2001, **35**, 2369.
46. G. Marbán and A. B. Fuertes, *Catal. Lett.*, 2002, **84**, 13.
47. N. Apostolescu, B. Geiger, K. Hizbullah, M. T. Jan, S. Kureti, D. Reichert, F. Schott and W. Weisweiler, *Appl. Catal. B: Environ.*, 2006, **62**, 104.
48. F. Nakajima and I. Hamada, *Catal. Today*, 1996, **29**, 109.
49. S. Roy, B. Viswanath, M. S. Hegde and G. Madras, *J. Phys. Chem. C*, 2008, **112**, 6002.
50. L. Ma, J. Li, R. Ke and L. Fu, *J. Phys. Chem. C*, 2011, **115**, 7603.
51. F. Liu, H. He and C. Zhang, *Chem. Commun.*, 2008, 2043.
52. F. Liu, H. He, C. Zhang, Z. Feng, L. Zheng, Y. Xie and T. Hu, *Appl. Catal. B: Environ.*, 2010, **96**, 408.
53. F. Liu, K. Asakura, P. Xie, J. Wang and H. He, *Catal. Today*, 2013, **201**, 131.
54. F. Liu, K. Asakura, H. He, Y. Liu, W. Shan, X. Shi and C. Zhang, *Catal. Today*, 2011, **164**, 520.
55. F. Liu, H. He, C. Zhang, W. Shan and X. Shi, *Catal. Today*, 2011, **175**, 18.
56. F. Liu and H. He, *J. Phys. Chem. C*, 2010, **114**, 16929.
57. F. Liu, H. He, Y. Ding and C. Zhang, *Appl. Catal. B: Environ.*, 2009, **93**, 194.
58. F. Liu, K. Asakura, H. He, W. Shan, X. Shi and C. Zhang, *Appl. Catal. B: Environ.*, 2011, **103**, 369.
59. F. Liu and H. He, *Catal. Today*, 2010, **153**, 70.
60. S. Yang, J. Li, C. Wang, J. Chen, L. Ma, H. Chang, L. Chen, Y. peng and N. Yan, *Appl. Catal. B: Environ.*, 2012, **117–118**, 73.
61. L. Chen, J. Li and M. Ge, *Environ. Sci. Technol.*, 2010, **44**, 9590.
62. Z. Si, D. Weng, X. Wu, J. Li and G. Li, *J. Catal.*, 2010, **271**, 43.
63. X. Mou, Y. Li, B. Zhang, L. Yao, X. Wei, D. S. Su and W. Shen, *Eur. J. Inorg. Chem.*, 2012, **2012**, 2684.
64. X.-Y. Yang, L. Sun, Z.-W. Huang, X.-M. Cheng, T.-W. Zhang, B. Li and X.-F. Tang, *Acta Phys. -Chim. Sin.*, 2012, **28**, 184.
65. X. Mou, B. Zhang, Y. Li, L. Yao, X. Wei, D. S. Su and W. Shen, *Angew. Chem. Int. Ed.*, 2012, **51**, 2989.
66. L. Chen, J. Li and M. Ge, *J. Phys. Chem. C*, 2009, **113**, 21177.
67. R. Q. Long and R. T. Yang, *J. Am. Chem. Soc.*, 1999, **121**, 5595.
68. G. Carja, G. Delahay, C. Signorile and B. Coq, *Chem. Commun.*, 2004, 1404.
69. Z. Wu, R. Jin, Y. Liu and H. Wang, *Catal. Commun.*, 2008, **9**, 2217.
70. Z. Wu, R. Jin, H. Wang and Y. Liu, *Catal. Commun.*, 2009, **10**, 935.
71. Y. Li, H. Cheng, D. Li, Y. Qin, Y. Xie and S. Wang, *Chem. Commun.*, 2008, 1470.
72. W. Xu, Y. Yu, C. Zhang and H. He, *Catal. Commun.*, 2008, **9**, 1453.
73. X. Gao, Y. Jiang, Y. Zhong, Z. Luo and K. Cen, *J. Hazard. Mater.*, 2010, **174**, 734.
74. X. Gao, Y. Jiang, Y. Fu, Y. Zhong, Z. Luo and K. Cen, *Catal. Commun.*, 2010, **11**, 465.
75. W. Xu, H. He and Y. Yu, *J. Phys. Chem. C*, 2009, **113**, 4426.
76. W. Shan, F. Liu, H. He, X. Shi and C. Zhang, *ChemCatChem*, 2011, **3**, 1286.
77. W. Shan, F. Liu, H. He, X. Shi and C. Zhang, *Catal. Today*, 2012, **184**, 160.
78. W. Shan, F. Liu, H. He, X. Shi and C. Zhang, *Appl. Catal. B: Environ.*, 2012, **115–116**, 100.
79. L. Chen, J. Li, M. Ge and R. Zhu, *Catal. Today*, 2010, **153**, 77.
80. W. Shan, F. Liu, H. He, X. Shi and C. Zhang, *Chem. Commun.*, 2011, **47**, 8046.
81. L. Chen, J. Li, W. Ablikim, J. Wang, H. Chang, L. Ma, J. Xu, M. Ge and H. Arandiyan, *Catal. Lett.*, 2011, **141**, 1859.
82. Y. Peng, J. Li, L. Chen, J. Chen, J. Han, H. Zhang and W. Han, *Environ. Sci. Technol.*, 2012, **46**, 2864.
83. Y. Peng, Z. Liu, X. Niu, L. Zhou, C. Fu, H. Zhang, J. Li and W. Han, *Catal. Commun.*, 2012, **19**, 127.
84. L. Chen, J. Li, M. Ge, L. Ma and H. Chang, *Chin. J. Catal.*, 2011, **32**, 836.
85. Y. Shen, S. Zhu, T. Qiu and S. Shen, *Catal. Commun.*, 2009, **11**, 20.
86. L. Zhu, B. Huang, W. Wang, Z. Wei and D. Ye, *Catal. Commun.*, 2011, **12**, 394.
87. X. Chen, S. Gao, H. Wang, Y. Liu and Z. Wu, *Catal. Commun.*, 2011, **14**, 1.
88. F. Li, Y. Zhang, D. Xiao, D. Wang, X. Pan and X. Yang, *ChemCatChem*, 2010, **2**, 1416.
89. H. Wang, X. Chen, X. Weng, Y. Liu, S. Gao and Z. Wu, *Catal. Commun.*, 2011, **12**, 1042.
90. X. Chen, H. Wang, Z. Wu, Y. Liu and X. Weng, *J. Phys. Chem. C*, 2011, **115**, 17479.
91. Z. Ma, D. Weng, X. Wu and Z. Si, *J. Environ. Sci.*, 2012, **24**, 1305.
92. T. Gu, Y. Liu, X. Weng, H. Wang and Z. Wu, *Catal. Commun.*, 2010, **12**, 310.
93. Z. Si, D. Weng, X. Wu, J. Yang and B. Wang, *Catal. Commun.*, 2010, **11**, 1045.
94. Z. Si, D. Weng, X. Wu, R. Ran and Z. Ma, *Catal. Commun.*, 2012, **17**, 146.
95. A. Z. Ma and W. Grunert, *Chem. Commun.*, 1999, 71.
96. R. Q. Long and R. T. Yang, *Catal. Lett.*, 2001, **74**, 201.
97. M. Schwidder, S. Heikens, A. De Toni, S. Geisler, M. Berndt, A. Brückner and W. Grünert, *J. Catal.*, 2008, **259**, 96.
98. M. Iwasaki, K. Yamazaki, K. Banno and H. Shinjoh, *J. Catal.*, 2008, **260**, 205.
99. S. Brandenberger, O. Kröcher, A. Tissler and R. Althoff, *Appl. Catal. B: Environ.*, 2010, **95**, 348.
100. M. Høj, M. J. Beier, J.-D. Grunwaldt and S. Dahl, *Appl. Catal. B: Environ.*, 2009, **93**, 166.
101. M. Schwidder, M. S. Kumar, A. Bruckner and W. Grunert, *Chem. Commun.*, 2005, 805.

102. M. Devadas, O. Krocher, M. Elsener, A. Wokaun, G. Mitrikas, N. Soger, M. Pfeifer, Y. Demel and L. Mussmann, *Catal. Today*, 2007, **119**, 137.
103. S. Brandenberger, O. Kröcher, A. Tissler and R. Althoff, *Ind. Eng. Chem. Res.*, 2011, **50**, 4308.
104. M. Iwasaki, K. Yamazaki and H. Shinjoh, *Appl. Catal. B: Environ.*, 2011, **102**, 302.
105. G. Qi, Y. Wang and R. Yang, *Catal. Lett.*, 2008, **121**, 111.
106. R. Q. Long and R. T. Yang, *J. Catal.*, 1999, **188**, 332.
107. R. Q. Long and R. T. Yang, *J. Catal.*, 2002, **207**, 224.
108. M. Schwidder, M. Santhosh Kumar, U. Bentrup, J. Pérez-Ramírez, A. Brückner and W. Grünert, *Micropor. Mesopor. Mater.*, 2008, **111**, 124.
109. M. Li, Y. Yeom, E. Weitz and W. Sachtler, *Catal. Lett.*, 2006, **112**, 129.
110. A. Savara, M.-J. Li, W. M. H. Sachtler and E. Weitz, *Appl. Catal. B: Environ.*, 2008, **81**, 251.
111. S. Brandenberger, O. Kröcher, A. Wokaun, A. Tissler and R. Althoff, *J. Catal.*, 2009, **268**, 297.
112. D. Klukowski, P. Balle, B. Geiger, S. Wagloehner, S. Kureti, B. Kimmerle, A. Baiker and J. D. Grunwaldt, *Appl. Catal. B: Environ.*, 2009, **93**, 185.
113. C. He, Y. Wang, Y. Cheng, C. K. Lambert and R. T. Yang, *Appl. Catal. A: Gen.*, 2009, **368**, 121.
114. S. Brandenberger, O. Kröcher, M. Casapu, A. Tissler and R. Althoff, *Appl. Catal. B: Environ.*, 2011, **101**, 649.
115. X. Shi, F. Liu, W. Shan and H. He, *Chin. J. Catal.*, 2012, **33**, 454.
116. L. Ma, J. Li, H. Arandiyan, W. Shi, C. Liu and L. Fu, *Catal. Today*, 2012, **184**, 145.
117. M. Iwasaki and H. Shinjoh, *Chem. Commun.*, 2011, **47**, 3966.
118. I. Heo, Y. Lee, I.-S. Nam, J. W. Choung, J.-H. Lee and H.-J. Kim, *Micropor. Mesopor. Mater.*, 2011, **141**, 8.
119. J. Li, R. Zhu, Y. Cheng, C. K. Lambert and R. T. Yang, *Environ. Sci. Technol.*, 2010, **44**, 1799.
120. L. Ma, J. Li, Y. Cheng, C. K. Lambert and L. Fu, *Environ. Sci. Technol.*, 2012, **46**, 1747.
121. J. Li, H. Chang, L. Ma, J. Hao and R. T. Yang, *Catal. Today*, 2011, **175**, 147.
122. B. Moden, J. Donohue, W. Cormier and H.-X. Li, *Top. Catal.*, 2010, **53**, 1367.
123. G. Qi and R. T. Yang, *Catal. Lett.*, 2005, **100**, 243.
124. A. Grossale, I. Nova, E. Tronconi, D. Chatterjee and M. Weibel, *J. Catal.*, 2008, **256**, 312.
125. M. Devadas, O. Kröcher, M. Elsener, A. Wokaun, N. Söger, M. Pfeifer, Y. Demel and L. Mussmann, *Appl. Catal. B: Environ.*, 2006, **67**, 187.
126. P. Forzatti, I. Nova and E. Tronconi, *Angew. Chem. Int. Ed.*, 2009, **121**, 8516.
127. P. Kern, M. Klimczak, T. Heinzelmann, M. Lucas and P. Claus, *Appl. Catal. B: Environ.*, 2010, **95**, 48.
128. J. Baik, S. Yim, I.-S. Nam, Y. Mok, J.-H. Lee, B. Cho and S. Oh, *Top. Catal.*, 2004, **30-31**, 37.
129. H. Sjövall, L. Olsson, E. Fridell and R. J. Blint, *Appl. Catal. B: Environ.*, 2006, **64**, 180.
130. M. Berggrund, H. Ingelsten, M. Skoglundh and A. Palmqvist, *Catal. Lett.*, 2009, **130**, 79.
131. J.-H. Park, H. J. Park, J. H. Baik, I.-S. Nam, C.-H. Shin, J.-H. Lee, B. K. Cho and S. H. Oh, *J. Catal.*, 2006, **240**, 47.
132. T. Komatsu, M. Nunokawa, I. S. Moon, T. Takahara, S. Namba and T. Yashima, *J. Catal.*, 1994, **148**, 427.
133. G. Delahay, S. Kieger, N. Tanchoux, P. Trens and B. Coq, *Appl. Catal. B: Environ.*, 2004, **52**, 251.
134. N. Wilken, K. Wijayanti, K. Kamasamudram, N. W. Currier, R. Vedaiyan, A. Yezerets and L. Olsson, *Appl. Catal. B: Environ.*, 2012, **111–112**, 58.
135. C. H. F. Peden, J. H. Kwak, S. D. Burton, R. G. Tonkyn, D. H. Kim, J.-H. Lee, H.-W. Jen, G. Cavataio, Y. Cheng and C. K. Lambert, *Catal. Today*, 2012, **184**, 245.
136. B. Moden, J. M. Donohue, W. E. Cormier and H. X. Li, in *Studies in Surface Science and Catalysis*, eds. P. M. Antoine Gédéon and B. Florence, Elsevier, 2008, **74**, 1219.
137. T. Nanba, A. Sultana, S. Masukawa, M. Haneda, J. Uchisawa, A. Obuchi and H. Hamada, *Top. Catal.*, 2009, **52**, 1766.
138. A. Sultana, T. Nanba, M. Haneda and H. Hamada, *Catal. Commun.*, 2009, **10**, 1859.
139. A. Sultana, T. Nanba, M. Sasaki, M. Haneda, K. Suzuki and H. Hamada, *Catal. Today*, 2011, **164**, 495.
140. J. H. Kwak, D. Tran, S. D. Burton, J. Szanyi, J. H. Lee and C. H. F. Peden, *J. Catal.*, 2012, **287**, 203.
141. J. H. Kwak, R. G. Tonkyn, D. H. Kim, J. Szanyi and C. H. F. Peden, *J. Catal.*, 2010, **275**, 187.
142. D. W. Fickel, E. D'Addio, J. A. Lauterbach and R. F. Lobo, *Appl. Catal. B: Environ.*, 2011, **102**, 441.
143. S. J. Schmieg, S. H. Oh, C. H. Kim, D. B. Brown, J. H. Lee, C. H. F. Peden and D. H. Kim, *Catal. Today*, 2012, **184**, 252.
144. D. W. Fickel and R. F. Lobo, *J. Phys. Chem. C*, 2010, **114**, 1633.
145. S. T. Korhonen, D. W. Fickel, R. F. Lobo, B. M. Weckhuysen and A. M. Beale, *Chem. Commun.*, 2011, **47**, 800.
146. U. Deka, A. Juhin, E. A. Eilertsen, H. Emerich, M. A. Green, S. T. Korhonen, B. M. Weckhuysen and A. M. Beale, *J. Phys. Chem. C*, 2012, **116**, 4809.
147. V. F. Kispersky, A. J. Kropf, F. H. Ribeiro and J. T. Miller, *Phys. Chem. Chem. Phys.*, 2012, **14**, 2229.
148. J. S. McEwen, T. Anggara, W. F. Schneider, V. F. Kispersky, J. T. Miller, W. N. Delgass and F. H. Ribeiro, *Catal. Today*, 2012, **184**, 129.
149. J. Hun Kwak, H. Zhu, J. H. Lee, C. H. F. Peden and J. Szanyi, *Chem. Commun.*, 2012, **48**, 4758.
150. J. Kwak, D. Tran, J. Szanyi, C. Peden and J. Lee, *Catal. Lett.*, 2012, **142**, 295.
151. M. Moliner, C. Franch, E. Palomares, M. Grill and A. Corma, *Chem. Commun.*, 2012, **48**, 8264.
152. S. I. Zones, *J. Chem. Soc., Faraday Trans.*, 1991, **87**, 3709.
153. L. Ren, Y. Zhang, S. Zeng, L. Zhu, Q. Sun, H. Zhang, C. Yang, X. Meng, X. Yang and F.-S. Xiao, *Chin. J. Catal.*, 2012, **33**, 92.
154. L. Ren, L. Zhu, C. Yang, Y. Chen, Q. Sun, H. Zhang, C. Li, F. Nawaz, X. Meng and F.-S. Xiao, *Chem. Commun.*, 2011, **47**, 9789.
155. A. Lorena Picone, S. J. Warrender, A. M. Z. Slawin, D. M. Dawson, S. E. Ashbrook, P. A. Wright, S. P. Thompson, L. Gaberova, P. L. Llewellyn, B. Moulin, A. Vimont, M. Daturi, M. B. Park, S. K. Sung, I.-S. Nam and S. B. Hong, *Micropor. Mesopor. Mater.*, 2011, **146**, 36.
156. U. Deka, I. Lezcano-Gonzalez, S. J. Warrender, A. Lorena Picone, P. A. Wright, B. M. Weckhuysen and A. M. Beale, *Micropor. Mesopor. Mater.*, 2013, **166**, 144.
157. J. Lee, S. Song and K. M. Chun, *Ind. Eng. Chem. Res.*, 2010, **49**, 3553.
158. T. Miyadera, *Appl. Catal. B: Environ.*, 1993, **2**, 199.
159. K.-I. Shimizu, M. Tsuzuki and A. Satsuma, *Appl. Catal. B: Environ.*, 2007, **71**, 80.
160. H. He, X. Zhang, Q. Wu, C. Zhang and Y. Yu, *Catal. Surv. Asia*, 2008, **12**, 38.
161. Q. Wu, H. He and Y. Yu, *Appl. Catal. B: Environ.*, 2005, **61**, 107.
162. Y. Yu, H. He, Q. Feng, H. Gao and X. Yang, *Appl. Catal. B: Environ.*, 2004, **49**, 159.
163. Y. Yu, X. Song and H. He, *J. Catal.*, 2010, **271**, 343.
164. Y. Li, X. Zhang, H. He, Y. Yu, T. Yuan, Z. Tian, J. Wang and Y. Li, *Appl. Catal. B: Environ.*, 2009, **89**, 659.
165. Y. Yan, Y. Yu, H. He and J. Zhao, *J. Catal.*, 2012, **293**, 13.
166. H. Gao, T. Yan, Y. Yu and H. He, *J. Phys. Chem. C*, 2008, **112**, 6933.
167. T. Miyadera, *Appl. Catal. B: Environ.*, 1997, **13**, 157.
168. W. L. Johnson II, G. B. Fisherb and T. J. Toops, *Catal. Today* 2012, **184**, 166.
169. Y. H. Yeom, M. Li, W. M. H. Sachtler and E. Weitz, *J. Catal.*, 2007, **246**, 413.
170. T. Chafik, S. Kameoka, Y. Ukisu and T. Miyadera, *J. Mol. Catal. A: Chem.*, 1998, **136**, 203.
171. A. Martínez-Arias, D. Gamarra, M. Fernández-García, A. Hornés, P. Bera, Z. Koppány and Z. Schay, *Catal. Today*, 2009, **143**, 211.
172. Y. Yu, H. He and Q. Feng, *J. Phys. Chem. B*, 2003, **107**, 13090.
173. Y. B. Yu, H. W. Gao and H. He, *Catal. Today*, 2004, **93–95**, 805.

174. P. J. Linstrom and W. G. Mallard, *NIST Chemistry Webbook*, 2003, NIST Standard Reference Database Number 69, http://webbook.nist.gov.
175. M. El-Maazawi, A. N. Finken, A. B. Nair and V. H. Grassian, *J. Catal.*, 2000, **191**, 138.
176. A. Panov and J. J. Fripiat, *Langmuir*, 1998, **14**, 3788.
177. M. I. Zaki, M. A. Hasan, F. A. Al-Sagheer and L. Pasupulety, *Langmuir*, 1999, **16**, 430.
178. S. Chansai, R. Burch, C. Hardacre, J. Breen and F. Meunier, *J. Catal.*, 2010, **276**, 49.
179. H. Gao, H. He, Y. Yu and Q. Feng, *J. Phys. Chem. B*, 2005, **109**, 13291.
180. S. T. Korhonen, A. M. Beale, M. A. Newton and B. M. Weckhuysen, *J. Phys. Chem. C*, 2010, **115**, 885.
181. F. C. Meunier, J. P. Breen, V. Zuzaniuk, M. Olsson and J. R. H. Ross, *J. Catal.*, 1999, **187**, 493.
182. X. She and M. Flytzani-Stephanopoulos, *J. Catal.*, 2006, **237**, 79.
183. K.-I. Shimizu, M. Tsuzuki, K. Kato, S. Yokota, K. Okumura and A. Satsuma, *J. Phys. Chem. C*, 2006, **111**, 950.
184. A. Sultana, M. Haneda, T. Fujitani and H. Hamada, *Catal. Lett.*, 2007, **114**, 96.
185. H. He, Y. Li, X. Zhang, Y. Yu and C. Zhang, *Appl. Catal. A: Gen.*, 2010, **375**, 258.
186. Q. Wu, Y. Yu and H. He, *Chin. J. Catal.*, 2006, **27**, 993.
187. Q. Wu, H. Gao and H. He, *Chin. J. Catal.*, 2006, **27**, 403.
188. A. Takahashi, M. Haneda, T. Fujitani and H. Hamada, *J. Mol. Catal. A: Chem.*, 2007, **261**, 6.
189. Q. Yu, X. Wang, N. Xing, H. Yang and S. Zhang, *J. Catal.*, 2007, **245**, 124.
190. C. A. Taatjes, N. Hansen, A. McIlroy, J. A. Miller, J. P. Senosiain, S. J. Klippenstein, F. Qi, L. Sheng, Y. Zhang, T. A. Cool, J. Wang, P. R. Westmoreland, M. E. Law, T. Kasper and K. Kohse-Höinghaus, *Science*, 2005, **308**, 1887.
191. N. Bion, J. Saussey, M. Haneda and M. Daturi, *J. Catal.*, 2003, **217**, 47.
192. N. Bion, J. Saussey, C. Hedouin, T. Seguelong and M. Daturi, *Phys. Chem. Chem. Phys.*, 2001, **3**, 4811.
193. R. M. Ferullo, M. M. Branda, G. R. Garda and N. J. Castellani, *J. Mol. Catal. A: Chem.*, 2001, **167**, 115.
194. H. Gao and H. He, *Spectrochim. Acta A*, 2005, **61**, 1233.
195. S. Tamm, H. H. Ingelsten and A. E. C. Palmqvist, *J. Catal.*, 2008, **255**, 304.
196. F. Thibault-Starzyk, E. Seguin, S. Thomas, M. Daturi, H. Arnolds and D. A. King, *Science*, 2009, **324**, 1048.
197. Y. Ukisu, S. Sato, A. Abe and K. Yoshida, *Appl. Catal. B: Environ.*, 1993, **2**, 147.
198. Y. Ukisu, T. Miyadera, A. Abe and K. Yoshida, *Catal. Lett.*, 1996, **39**, 265.
199. S. Kameoka, T. Chafik, Y. Ukisu and T. Miyadera, *Catal. Lett.*, 1998, **55**, 211.
200. S. Chansai, R. Burch, C. Hardacre, J. Breen and F. Meunier, *J. Catal.*, 2011, **281**, 98.
201. V. Zuzaniuk, F. C. Meunier and J. R. H. Ross, *J. Catal.*, 2001, **202**, 340.
202. R. Rathore and J. K. Kochi, *J. Org. Chem.*, 1996, **61**, 627.
203. M. B. Smith and J. March, *March's Advanced Organic Chemistry Reactions, Mechanisms, and Structure, Sixth Edition*, 2007, Wiley-Interscience A John Wiley & Sons, Inc., 784.
204. D. L. H. Williams, *Advances in Physical Organic Chemistry 19 (Edited by V. Gold and D. Bethell)*, 1983, Academic Press Inc., New York, 381.
205. A. Obuchi, C. Wögerbauer, R. Köppel and A. Baiker, *Appl. Catal. B: Environ.*, 1998, **19**, 9.
206. H. He, Y. Yu, Y. Li, Q. Wu, X. Zhang, C. Zhang, X. Shi and X. Song, *Chin. J. Catal.* , 2010, **31**, 491.
207. F. C. Meunier and J. R. H. Ross, *Appl. Catal. B: Environ.*, 2000, **24**, 23.
208. Q. Wu, H. Gao and H. He, *J. Phys. Chem. B*, 2006, **110**, 8320.
209. R. Burch, J. Breen, C. Hill, B. Krutzsch, B. Konrad, E. Jobson, L. Cider, K. Eränen, F. Klingstedt and L. E. Lindfors, *Top. Catal.*, 2004, **30-31**, 19.
210. M. Richter, U. Bentrup, R. Eckelt, M. Schneider, M. M. Pohl and R. Fricke, *Appl. Catal. B: Environ.*, 2004, **51**, 261.
211. S. Satokawa, *Chem Lett.*, 2000, **29**, 294.
212. J. P. Breen, R. Burch, C. Hardacre, C. J. Hill and C. Rioche, *J. Catal.*, 2007, **246**, 1.
213. X. Zhang, H. He and Z. Ma, *Catal. Commun.*, 2007, **8**, 187.
214. X. Zhang, Y. Yu and H. He, *Appl. Catal. B: Environ.*, 2007, **76**, 241.
215. K. Eränen, F. Klingstedt, K. Arve, L.-E. Lindfors and D. Y. Murzin, *J. Catal.*, 2004, **227**, 328.
216. K. Eränen, L.-E. Lindfors, F. Klingstedt and D. Y. Murzin, *J. Catal.*, 2003, **219**, 25.
217. X. Shi, Y. Yu, H. He, S. Shuai, H. Dong and R. Li, *J. Environ. Sci.*, 2008, **20**, 177.
218. X. P. Song, C. B. Zhang and H. He, *Chin. J. Catal.*, 2008, **29**, 524.
219. Y. Li and F. Qi, *Accounts Chem. Res.*, 2009, **43**, 68.